INVESTIGATION OF AN INVESTMENT CASTING METHOD COMBINED WITH ADDITIVE MANUFACTURING METHODS FOR MANUFACTURING LATTICE STRUCTURES

Ganapathy D. Kodira

Thesis Prepared for the Degree of

MASTER OF SCIENCE

UNIVERSITY OF NORTH TEXAS

August 2013

APPROVED:

Jaehyung Ju, Major Professor
Tae-Youl Choi, Co-Major Professor
Nandika A, D'souza, Committee Member
Yong Tao, Chair of the Department of Mechanical and Energy Engineering
Costas Tsatoulis, Dean of the College of Engineering
Mark Wardell, Dean of the Toulouse Graduate School

Kodira, Ganapathy D. Investigation of an investment casting method combined with additive manufacturing methods for manufacturing lattice structures. Master of Science (Mechanical and Energy Engineering), August 2013, 5 tables, 31 figures, bibliography, 37 titles.

Cellular metals exhibit combinations of mechanical, thermal and acoustic properties that provide opportunities for various implementations and applications; light weight aerospace and automobile structures, impact and noise absorption, heat dissipation, and heat exchange. Engineered cell topologies enable one to control mechanical, thermal, and acoustic properties of the gross cell structures. A possible way to manufacture complex 3D metallic cellular solids for mass production with a relatively low cost, the investment casting (IC) method may be used by combining the rapid prototyping (RP) of wax or injection molding. In spite of its potential to produce mass products of various 3D cellular metals, the method is known to have significant casting porosity as a consequence of the complex cellular topology which makes continuous fluid's access to the solidification interface difficult. The effects of temperature on the viscosity of the fluids were studied. A comparative cost analysis between AM-IC and additive manufacturing methods is carried out. In order to manufacture 3D cellular metals with various topologies for multi-functional applications, the casting porosity should be resolved. In this study, the relations between casting porosity and processing conditions of molten metals while interconnecting with complex cellular geometries are investigated. Temperature and pressure conditions on the rapid prototyping – investment casting (RP-IC) method are reported, thermal stresses induced are also

studied. The manufactured samples are compared with those made by additive manufacturing methods.

ACKNOWLEDGEMENTS

I would like to extend my sincere gratitude and appreciation to my adviser, Dr. Ju,Jaehyung for his support, understanding, and constructive guidance. It is my privilege to have the opportunity to work with Dr.Ju. It was his encouragement, integrity and understanding that got me this far. DrJu has treated me like a family member, for which I am ever so grateful.

I also want to thank my Co-advisor. Dr. Tae-Youl Choi, for encouraging me to be innovative and for granting me access to the instruments from his laboratory. Also, my gratitude goes to Dr. Richard F.Reidy for granting me permission to use his laboratory equipment. My sincere appreciation also extends to the members of my master thesis committee - Dr. Ju, Jaehyung, Dr. Choi, Tae-Youl, Dr. D'souza, Nandika Anne - for their committed service and support, their ideas, and suggestions that helped improve my work significantly.

I would like to thank Mr. Brian Bass of the Fort Worth Aluminum Foundry, Inc for allowing me to use their facility, resources and also in assisting me carry out my experiments. I would like to specially thank my colleagues for assisting me with my work.

I want to express my thanks to all other faculty members and classmates in the Mechanical and Energy Engineering Department for their assistance and excellent lectures which have helped me in becoming a better professional.

Last but not the least; I wish to extend my gratitude to my parents for their unconditional love, patience and support.

TABLE OF CONTENTS

Page

LIST OF TABLES

Page

LIST OF FIGURES

Page

CHAPTER 1

INTRODUCTION

Investment casting has been around for generations and has found applications in numerous fields. An economic bulk manufacturing process, investment casting (IC) allows the manufacturer to easily adhere to design specifications. Now with the development of the additive manufacturing method (AMM), I aim to investigate the casting defects that arise from using sacrificial patterns developed from AMMs. This is done by combining AMM with investment casting, using an array of material as sacrificial patterns. In this study, the defects that arise throughout the investment casting process will be identified and attempt to resolve these defects in order to reduce the size of the final cast part, (i.e., the lattice core structure). Previous studies have identified some defects, such as misruns, cold shuts, inclusions, and shrinkage. In an attempt to eliminate these defects, this study investigated the effects of gate location optimization as a method to properly channel the flow of molten metals.

Ideally, this investigation will lead to the reduction of a number of casting defects that have typically arisen from the combination of investment casting and additive manufacturing methods. Optimization of gate location, selection of the appropriate material for the sacrificial pattern used, and utilization of an external pressure source are expected to improve the flow of the molten metals to all corners of the mold cavity prior to solidification; consequently, manufacturers will be able to cast with significantly improved accuracy.

1.1 Motivation of the Thesis

Cellular metals exhibit a combination of mechanical, thermal, and acoustic properties that provide opportunities for various implementations and applications; including light weight, aerospace and automobile structures, impact and noise absorption, heat dissipation, and heat exchange. Engineered cell topologies enable one to control mechanical, thermal, and acoustic properties of the gross cell structures. The combination of investment casting and Additive Manufacturing (AM) is one possible way to manufacture complex 3D metallic cellular solids for mass production at a relatively low cost. In spite of its potential to mass produce various 3D cellular metals, the method is known to have significant casting defects as a consequence of the complex cellular topology involved; such complexity often hinders continuous fluid access to the solidification interface. In order to manufacture 3D cellular metals with various topologies for multi-functional applications, the casting defects must be investigated and resolved.

1.2 Objectives

The castability of a metal alloy is its capacity to be cast into a particular shape using a given casting process. Their fluidity limits the castability of alloys and their final properties; as a result of this reduced fluidity, casting defects-such as misruns, cold shuts, porosity, inclusions, shrinkage, and poor surface finish-can occur. The main objective of this study is to investigate the casting defects that arise during the investment casting process as well as the sacrificial patterns developed from various additive manufacturing techniques used in the production of network lattice metals.

1.3 Thesis Outline

Chapter 2 provides a brief review of the relevant literature which encompasses additive manufacturing, investment casting and various methods used to manufacture cellular metals.

Chapter 3 outlines ananalytical approach to the fluid flow in order to estimate the velocity of the fluid at various points in the mold cavity and show the effect of temperature dependent viscosity on the flow velocity.

Chapter 4 discusses the experimental casting trials carried out and the hypothesis used to improve fluid flow.

Chapter 5 uses cost comparison to demonstrate the increased economic feasibility of the AM-IC process as compared to the EBM process.

Chapter 6 discusses manufacturing trial results, shell crack analysis, and the failures encountered in this study, as well as suggested improvements to ameliorate similar difficulties.

Chapter 7 characterizes material property and analyses the failure of the ceramic shell.

Chapter 8 lists the conclusions of the study; the chapter also discusses future work planned and offers possible concepts and ideas for future experiments to further develop the AM-IC process.

CHAPTER 2

LITERATURE REVIEW

This chapter gives a brief overview of the useful literature related to additive manufacturing method (AMM), investment casting process, and investment casting defects.

Investment casting (IC) is an industrial metal-forming process. Investment casting also goes by the name of precision casting or the lost-wax process. The IC process may be usefully divided into three main stages [1]:

a) Sacrificial patterns are produced using a die with materials such as wax, plastic, or other suitable materials. The pattern is a replica of the casting to be produced and includes allowances for the expansion and contraction which occur during the casting process. The patterns are then placed on a running system and passed through to the moulding stage.
b) The pattern assembly is coated with a suitable setting refractory mixture; traditionally slurry is used to produce a block or shell mold. When the mold sets, the pattern is removed either through melting or dissolution; consequently, what remains is a cavity which replicates the shape of the final cast product required.
c) The metal is cast into the mold and allowed to cool. Upon cooling, the mold is then broken and the cast part removed before it is further machined and processed to achieve the final part.

2.1 Factors Affecting Casting Process

Factors which highly influence the casting process are solidification of the molten metal, flow of the molten metal into the mold cavity, heat transfer during solidification

and the material used to develop the mold. It is essential to understand the effects of these factors [2].

2.1.1 Solidification of Metals

The solidification process for pure metals and alloys varies quite markedly; that is, pure metals solidify at a constant temperature whereas alloys solidify over a range of temperatures. Unlike alloys, pure metals have a well-defined freezing point, as the temperature of the molten metal drops to the freezing point the molten metal begins to solidify. Such solidification takes place at a constant temperature (isothermal process) as the heat is given off (latent heat of fusion) [2]. After a certain duration of time, the freezing ends and the molten metal is completely solidified.

The type of cast structure developed during solidification of alloys and pure metals depends on factors such as composition of a particular alloy, heat transfer rate, and velocity of flow of the molten metal.

Typically, the grain structures of a pure metal are columnar grains and equiaxed grains. The mold wall, being close to ambient temperature, is the region where the molten metal cools rapidly. This region is referred to as the chill zone, and it is where the casting develops a solidified skin of equiaxed grains. Columnar grains are those grains which grow in a favorable direction (i.e., in the direction opposite to the heat transfer from the mold). The grains that have a different orientation are blocked from further growth.

In order to improve the mechanical properties of pure metals, alloying techniques are used to enhance or modify the properties of the pure metal to increase its suitability for required applications. In the case of alloys, solidification begins as the temperature

drops below the liquidus with the completion of the process when the temperature reaches the solidus. In this temperature range, the alloy exists in a mushy or pasty state with columnar dendrites.

The solidification time can be obtained from Chvorinov's rule, a function of the volume of a casting and the surface area and it is given by:

$$Solidification\ Time = C\left(\frac{Volume}{Surface\ Area}\right)^{n}$$

Where:

C is a constant that reflect properties of the mold material, molten metal as well as the temperature.

$n$is a constant.

2.1.2 Fluid Flow and Heat Transfer

Another important parameter that influences the flow characteristics is Reynolds number, R_e, which is given by:

$$R_e = (vD\rho/\eta)$$

where:

v is the velocity of the liquid,

D diameter of the channel,

ρ is the density and η is the viscosity.

Reynolds number determines whether the flow of the fluid is laminar or turbulent. Typically, an R_e value up to 2,300 represents laminar flow, an R_e value of between 2,300 and 4,000 is considered a mixture of both laminar as well turbulent (this is an often encountered range in the casting process)[2],and an R_e value above 4,000 represents

turbulent flow. This often results in defects in the casting process, such as air entrapment and dross formation, the latter of which can be detrimental to the quality of the final cast part.

Other factors that affect fluidity include viscosity, surface tension, inclusions, mold material, design, and rate of pouring.

Because viscosity is a function of temperature, heat transfer directly affects the fluidity of the molten metal; additionally, the degree of superheat, or the increase of temperature beyond the melting point of an alloy, influences fluidity by delaying solidification.

Heat transfer during the casting process takes place througout the entire cycle- from pouring of the molten metal to solidification and cooling of the final cast part to room temperature. The heat transfer through the system varies based on several parameters. For instance, in regard to casting with thin-walled structures, the flow rate of the molten metal should be sufficiently high to prevent solidification due to a chilling - frequent occurrence as a result of the rapid drop in the fluid’s temperature upon its contact with the inner walls of the mold; this is dueto the temperature difference that exists between the molten metal and the mold walls.

2.3 Additive Manufacturing Technology

Additive manufacturing, more commonly referred to as 3D printing, is a process used to make solid, three-dimensional objects by using a digital 3D model. There is a sequence of eight steps required to develop a 3D model: [3]

1. Conceptualization and computer aided design (CAD)
2. Conversion to stereolithography (STL)

3. Transfer and manipulation of the STL file on the AM machine
4. Machine preparation
5. Part build
6. Part removal and cleanup
7. Post processing (removal of support structure)
8. Desired application

The general principle of additive manufacturing is a layer-by-layer deposition of the respective material being used to build the 3D part. Additive manufacturing uses CAD to design a soft copy of the 3D part; this corresponding CAD file is then converted to an STL file format, the first commercial additive manufacturing technology from 3D systems [3]. An STL file is used in order to define the CAD file based on its geometry by eliminating modeling history and any type of construction data that is associated with the imported file. Next, the STL file is sent to the 3D-printing machine where the file is analyzed and the printing process begins. The different types of printing processes is discussed in later chapters. Upon receiving the STL file, the 3D model is built layer-by-layer with a support material in order to provide the strength necessary for the entire part to be built. This build process is typically a fully-automated process which the machine will carry out itself. Immediately after the build process, the parts will be weak and will have support features on them which must be handled carefully during removal. After removal of the support structure, the part is ready to be used for its desired application which today extends to various disciplines.

Several printing technologies are available which differ in the method of material deposition. Certain technologies soften or melt the material to produce the layers,

whereas other technologies apply liquid materials which are cured using ultra-violet light. Some of the commonly used technologies include: [4]

- Stereolithography (SLA) - this process uses a laser beam in order to solidify and cure the plastic resin. DMS Somos®developed materials for 3D Systems QuickCast™ SLA process. The two materials developed for the SLA process areSomos® ProtoCast™ AF19120 and WaterShed™ 11120.
- Electron beam melting (EBM) - this is a direct CAD-to-metal rapid prototyping process for the manufacture of dense and porous metal parts. In EBM, the Ti6Al4V powder is melted layer-by-layer with an electron beam. The process uses an STL file of the part to be fabricated. Generated using a CAD software, Ti6Al4V is processed using Arcam AB (KrokslättsFabriker 27A SE-431 37 Mölndal Sweden) and is reported to have a yield strength of 910-940 MPa and ultimate tensile strength of 950-990 MPa[5]. Initial developments were carried out with iron-based metals, but the process has also been verified for tool steel, low alloy steel, alloyed titanium, commercially pure titanium, and nickel alloys. The current build volume which has been achieved is within a 200x200x160mm space [6].
- Selective laser sintering (SLS) - this process uses a high-powered laser beam to fuse small particles of plastic, metal, ceramic, or glass powders into the desired three-dimensional shapes. The laser selectively fuses powdered material by scanning the cross-section derived from the

description of the 3D digital part previously put into the system. The SLS machine typically uses a pulsed laser for this process. Some of the materials used to produce SLS patterns are nylon, glass-filled nylon, and the SLS specific SLS Flex (a flexible rubber-like material).

- Fused deposition modeling (FDM) - this is another method developed by Stratasys Corporation to aid the investment casting foundries. A specific type of wax material was developed by Stratasys for investment casting purposes; a second material option would beacrylonitrile butadiene styrene (ABS).
- 3D Inkjet printing (3DP) -Developed by 3D Systems, 3D inkjet printers are both compact and space efficient for offices or small workshops.These machines use a non-toxic wax which may be employed in the investment casting process.

Table 1: Available Additive Technologies and Their Corresponding Base Materials [7]

Additive Technologies	Base materials
Selective laser sintering (SLS)	Thermoplastic, ,metal powders, ceramic powders
Direct metal laser sintering (DMLS)	Any alloy metal
Fused deposition modeling (FDM)	Thermoplastic and eutectic metals
Stereolithography (SLA)	Photopolymer
Digital light processing (DLP)	Liquid resin
Fused filament fabrication (FFF)	PLA, ABS
Melted and extrusion modeling (MEM)	Metal wire, plastic filament
Selective heat sintering (SHS)	Thermoplastic powder
Electron beam melting (EBM)	Titanium alloys
Laminated object manufacturing (LOM)	Paper, foil, plastic film
Plaster based 3D Printing	Plastic, colored plaster

2.4 Photopolymerization Process

Photopolymerization is a process in which certain materials undergo solidification as a result of chemical change when exposed to a certain type of radiation. Various

types of radiation can be used to cure photopolymers, including gamma rays, ultraviolet light, X-rays, electron beams, and visible light.

Three configurations have been developed for the photopolymerization process: [3]

- Vector scan
- Mask projection
- Two-photon approach

The vector scan method is generally used in commercial STL machines which use a single laser to cure the layers being created on the build platform.

2.5 Additive Manufacturing – Capabilities, Limitations, and Cost

In order to ensure that a manufacturing process is both suitable and cost effective, several factors and process parameters must be taken into account. Some such factors include the labor intensity of the process as well as the cost of the equipment and auxiliary products. With increasing market demand for more complex and innovative parts, the flexibility of additive manufacturing makes it a viable option for the manufacture of such progressively complex geometries. Indeed, the many benefits associated with AMM, such as complexity-for-free manufacturing [8] have led to its ever increasing use of the process in the industry; however it has created a need for a fuller understanding of the capabilities and limitations of the AMM. With conventional machining, there is a direct relationship between the complexity of the geometry and the cost (i.e., cost tends to increase with increases in the complexity of the manufactured part).Conversely, additive manufacturing has no limitation in relation to complex geometry and does not require development of specialized tools.

The aforementioned heightened flexibility of AMM as compared to conventional machining can be seen in the manufacture of functional parts, such as rotating gears with meshing teeth and ball and socket joints, as well as manufacture of parts for assembly [8]. In conventional machining the unwanted material has to be cut or machined in order to realize the final part required, leading to notable material wastage; conversely, AM allows for materials to be placed only where necessary and thus utilizes the material more efficiently while enabling the manufacture of lattice structures and hollow parts in less time[9]. Because of this increase in efficiency and corresponding lack of investment in expensive tool development, AM allows manufacturers to substantially increase their rate of product dissemination in the market while simultaneously reducing the risk of early market placement.

When estimating the cost of the product, we must have a basis on which to calculate the cost. Important factors to be considered in our estimations include price competitiveness, profit margin, and the necessity of covering all costs in due time.

There are several methods used to determine the cost, and a number of corresponding uncertainties. These ambiguities are the result of the decisions which must to be made during the product development stage, such as selection of process parameters, material, and equipment selection, and the possibility of failure of the parameters. Currently, there are two approaches used in the estimation of product cost[10]: top-down approach and bottom-up approach.

The top-down approach involves cost estimation using product level information and does not require any detailed information about the design or manufacturing process, such as a bill of materials and material or assembly cost. On the other hand, the bottom-up approach uses information from the bill of materials, with the cost of each associated attribute being added up. Another frequently used cost estimation model is a metric-based economic viability evaluation model[11] to calculate the estimated cost of a product.

2.6 Manufacture of Cellular Metals and Investment Casting

Although rapid prototyping and other layer based manufacturing technologies have only been developed in recent years, systems using electron beams and lasers have revolutionized the manufacturing industry [12]. With the increasing application of cellular metals, several techniques have been developed and attempts made to manufacture these metals inexpensively. Those with relatively high densities, i.e., $\rho/\rho_s > 0.5$ (where ρ is the density of the cellular metal and ρ_s is the density of the solid from which it is made) [13], are made by solidification of metal alloys in entrapped gases. Panels have been fabricated from beryllium-copper alloys using rapid prototyping and investment casting[14]. Metallic lattice truss structures are usually made by perforating a metal sheet with a periodic diamond pattern with the sheets then folded at the nodes to make a 3D interconnected truss; however, because this method tends to result in poor utilization of the base plate material, pyramidal lattice truss structures with open cell configuration were developed from expanded metal sheets [15] and allow for 100 % utilization of material. The pyramidal core is stacked node-to-node and bonded together at these nodes to form a lattice block of cellular metals [16]. Several bonding methods,

such as brazing, resistance welding and gluing, are available and the methods vary depending on the type of material that must be bonded. Furthermore, various manufacturing processes are classified according to the state of matter in which the metal is processed (i.e., solid, liquid, and gaseous or ionized) [17].

Today, the investment casting process is frequently applied in the manufacture of metallic lattice structures when combined with AM processes, such as SLA, SLS, FDM and 3DP [4].

CHAPTER 3

MATHEMATICAL MODEL

3.1 Flow in Mold

Flow in the mold region during casting is of great importance as it influences many important phenomena, which have direct impact on the quality of the final cast part. These include flow and entrainment of the top surface, entrapment of subsurface inclusions and gas bubbles. Turbulent flow in the mold has been studied using plant measurements, water models and mathematical models. Owing to the similarity in kinematic viscosity of molten steel and water, water models have been extensively used in studying the flow of molten steel[18]. Several other methods such as the K-ε method which averages the effect of turbulence over both time and space using an increased effective viscosity field, several numerical models have been developed which satisfies mass momentum conservation in the computational domain by solving the conservative form of the Navier Stokes equation for isothermal incompressible Newtonian fluid and large eddy simulations (LES) which uses fine grid time steps to accurately calculate details of time dependent properties of flow [19]. Here we perform a numerical simulation to obtain the velocity and temperature profile with change in time. The governing equations used here are:

The continuity equation for an incompressible fluid in cylindrical coordinates is:

$$\frac{1}{r}\frac{\partial(ru_r)}{\partial r}+\frac{1}{r}\frac{\partial(u_\theta)}{\partial \theta}+\frac{\partial u_z}{\partial z}=0 \text{ …….(1)}$$

where $u_r, u_\theta and\ u_z$ are velocities in the$r$, θ and $z$direction, here we consider the velocity only in the z direction that is velocity u_z. Thus the momentum equation in the z direction is given by:

$$\rho\left(\frac{\partial u_z}{\partial t}+u_r\frac{\partial u_z}{\partial r}+\frac{u_\theta}{r}\frac{\partial u_z}{\partial \theta}+u_z\frac{\partial u_z}{\partial z}\right)=-\frac{\partial P}{\partial z}+\rho g_z+\mu\left[\frac{1}{r}\frac{\partial}{\partial r}\left(r\frac{\partial u_z}{\partial r}\right)+\frac{1}{r^2}\frac{\partial^2 u_z}{\partial \theta^2}+\frac{\partial^2 u_z}{\partial z^2}\right]\text{.....(2)}$$

In this study a 2 dimensional cast was considered, where the fluid velocity in the z direction is evaluated with respect to the r direction.As a result of which equation (2) reduces to the following:

$$\rho\frac{\partial u_z}{\partial t}=\frac{\partial P}{\partial z}+\rho g_z+\mu\frac{\partial^2 u_z}{\partial r^2}\text{.....(3)}$$

In order to obtain the velocity profile of u_z with respect to time and r equation [3] must be integrated, whereas obtaining a solution for equation (3) manually is not possible. As a result, a Matlab code is developed to solve the second order partial differential equation.

3.2 Analytical Approach of Fluid Flow

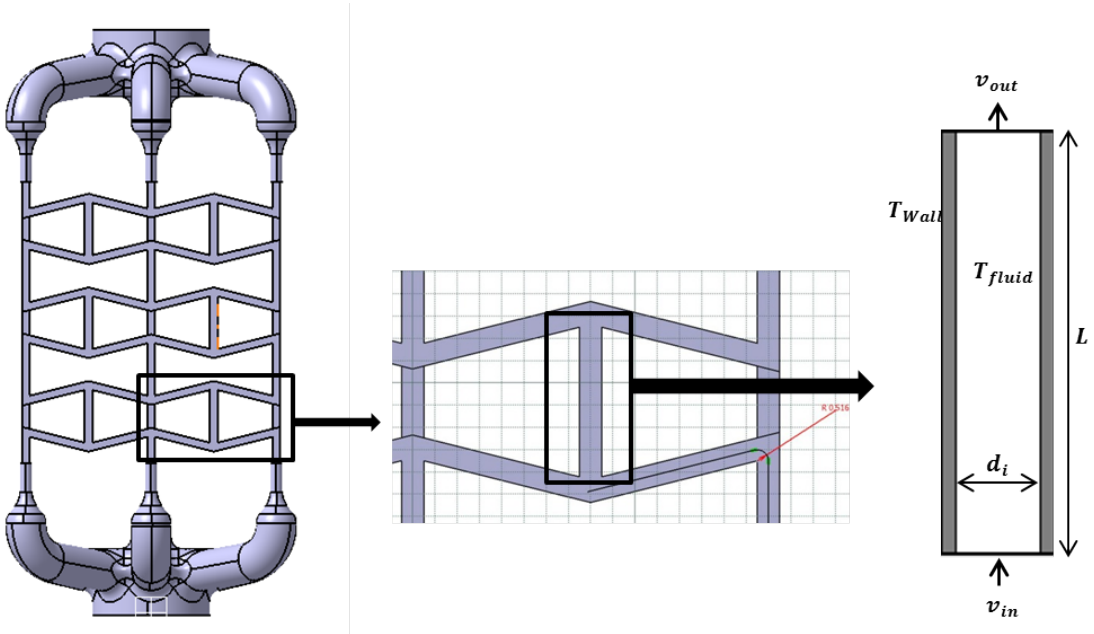

Figure 1: Sectional View of Flow Channel

A Matlab code is written to obtain the velocity profile of molten metal with time. Flow through the channel as shown in figure 1 is obtained. The diameter of the flow channel is 1 mm and the length is 100 mm, the temperature of the mold wall and fluid flowing through the channel are assumed to be the same. For this analytical approach several assumptions are established:

- Incompressible laminar flow
- Frictionless flow through channel
- Temperature along the inner and outer wall of the channel is the same
- Viscosity is a function of temperature
- Effects of surface tension and capillarity are negligible

Viscosity of molten aluminum varies as a function of temperature which is given by the equation, $-0.0143 * T + 12.81$[20].

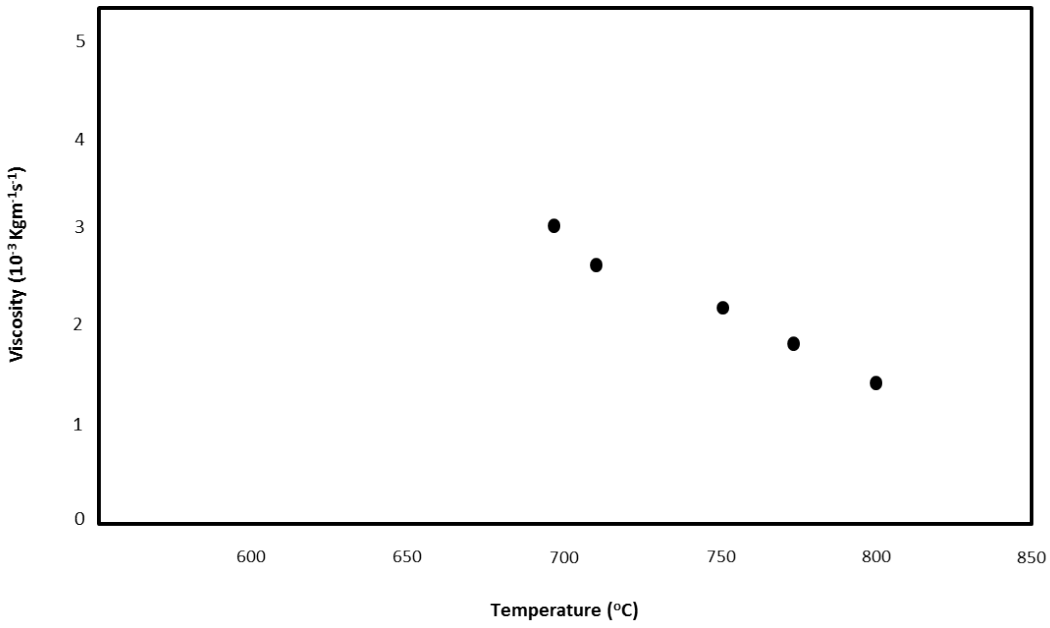

Figure 2: Temperature Dependent Viscosity of Aluminum (A356) Alloy [20]

The viscosity from figure 2 can be clearly seen to be a function of temperature and the with increasing the temperature of the molten aluminum alloy beyond its melting point upto about 800^{o}C, a steady reduction in viscosity of molten aluminum alloy (A356)is seen[20].The effects of surface tension and capillarity are negligible on a macro scale as the dominant forces acting are that of pressure and gravity [21]. However there is still a great uncertainty of the order of 25%, on the intrinsic value of aluminums surface tension. This uncertainty is due to the high sensitivity of the surface properties of molten aluminum to oxygen[22]. Large drop technique was employed to evaluate the surface tension of molten aluminum the test was performed in a high vacuum and high temperature atmosphere to promote de-oxidation of molten aluminum. The tests were carried out in graphite and alumina crucible.

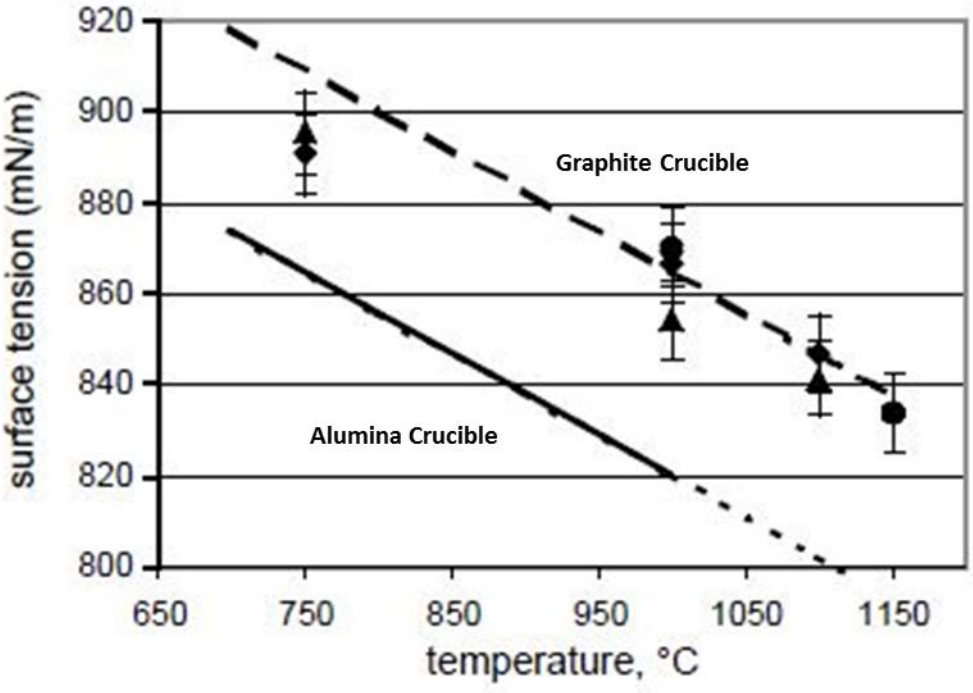

Figure 3: Surface Tension as a Function of Temperature [22]

Here pressure is the driving force and the pressure difference causes the fluid flow. The velocity profile for molten aluminum with increase in temperature is shown below.

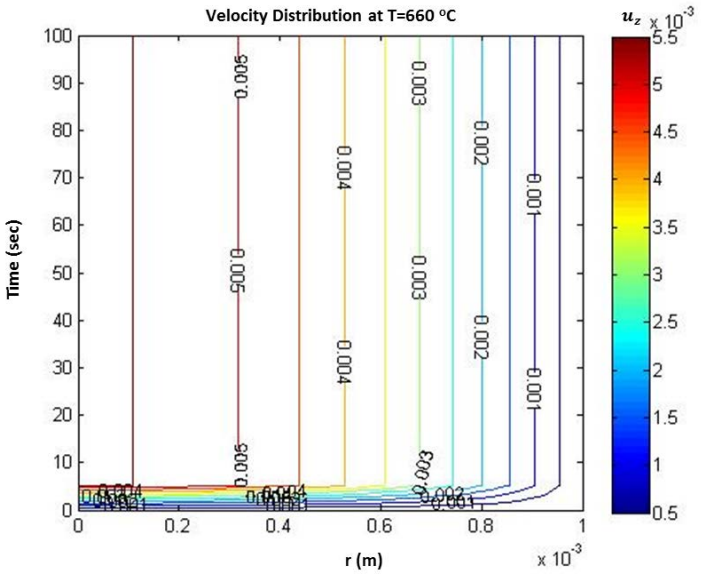

Figure 4: Velocity Profile for Molten Aluminum at 660 ^{o}C

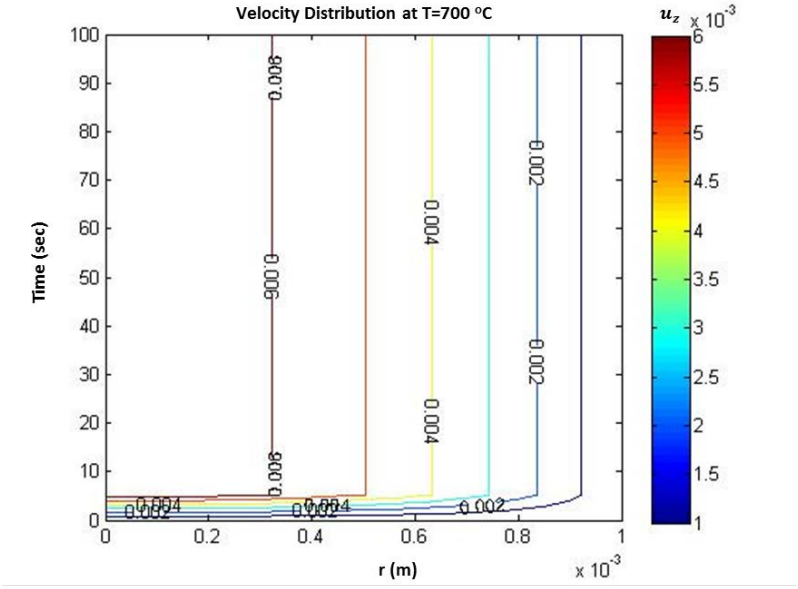

Figure 5: Velocity Profile for Molten Aluminum at 700 ^{o}C

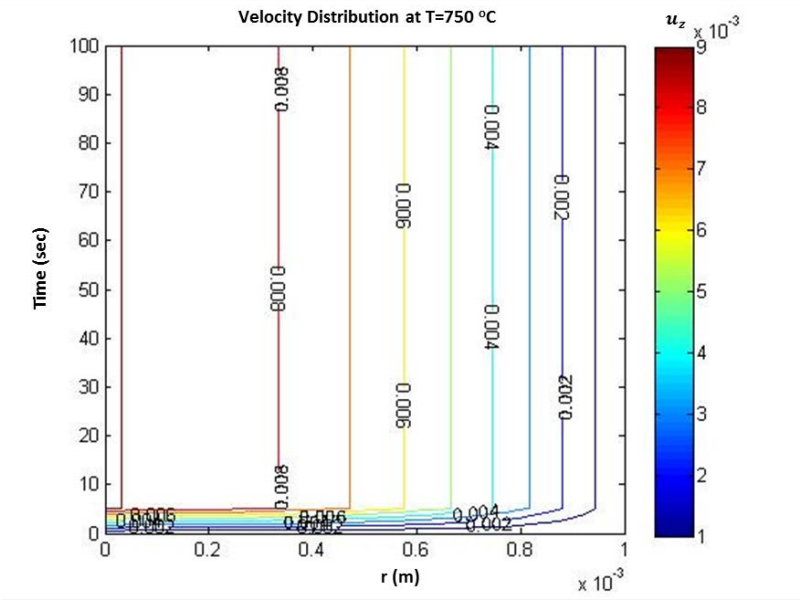

Figure 6: Velocity Profile for Molten Aluminum at 750 ^{o}C

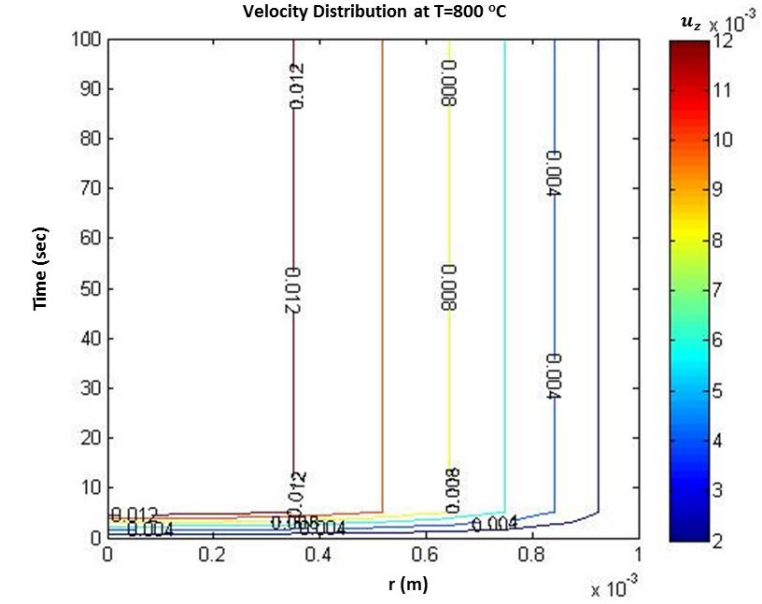

Figure 7: Velocity Profile for Molten Aluminum at 800 ^{o}C

Properties of aluminum considered to calculate the velocity profile are listed in table below.

Table 2: Properties Used for Molten Aluminum [23][24][25]

Molten Aluminum Properties	Unit
Liquid Density	$2685\ kg/m^3$
c_p(Specific Heat)	$910\ \mathrm{J/kg}.k$
Thermal Conductivity	$294\ w/m \cdot k$
Viscosity	$-0.0143 * T + 12.81$

Table 3: Properties Used for Silica Mold [26]

Silica Coating Shell Properties	Unit
Density	$2201\ kg/m^3$
c_p(Specific Heat)	$1297\mathrm{J/kg}.k$
Thermal Conductivity	$1.3\ w/m \cdot k$
Thickness of Casting	$6\ mm$
Heat Transfer Coefficient	$850\ W/m^2K$
Preheated temperature	$660\ ^oC - 800\ ^oC$

The velocity of molten aluminum depends on the viscosity and the viscosity is clearly a function of temperature, the viscosity of the molten metal decreases with increase in temperature and this will provide for better fluidity of the molten metal. In order to investigate the velocity distribution as a function of temperature-dependent viscosity for molten aluminum we consider a flow channel of 1 mm diameter and 100 mm length as shown in figure 1.For this analysis it must be noted that there is no change in the ceramic shell wall temperature, the ceramic shell is pre-heated to a temperature above 660^{o}C (melting point of aluminum) and is kept at this temperature. It can be seen from the velocity profile that the velocity of the molten metal increases with increase in temperature from 660^{o}C to 800^{o}C. Clearly showing that pre-heating the ceramic shell and elevating the temperature of the molten metal beyond its melting point will improve the fluidity of the molten metal. As the temperature of the molten metal begins to drop below 660oC the molten aluminum starts changing into a mushy paste, liquidus temperature for aluminum is 615^{o}C [27] and the flow becomes sluggish which reduces the flow velocity and this leads to defects in the final cast part, and the solidus temperature of aluminum being 555^{o}C[27] below the solidus temperature aluminum exists in a solid state.

CHAPTER 4

MANUFACTURING METHOD

In order to develop the sacrificial pattern using a 3D printer, a computer aided design (CAD) model of the pattern is first developed. This CAD model is then sent to the printer in a sterolithography (STL) format. The build time of the part is estimated by the machine based on the height of the build from the build platform; in order to minimize this build time, it must be taken care that the part is oriented in such a way that the height from the build platform is minimized. On completion of the build, the printed part will have to go through several post-processing steps. The printed part will adhere to the aluminum printing surface since the material jetted out from the nozzle is a liquid and is later cured and solidified by UV light. There are two ways of separating this printed part from the surface. First, the metal plate can be heated from below using a hot plate, a procedure that will melt the support material that is holding the part and until the plate together until the part can be slid off; this will require cleaning, as the melted wax will spread on the build plate and must be thoroughly cleaned before the next build to avoid unintentional alteration of the dimensions by the residual wax. Second, the plate and its associated parts can be placed in a freezer for about 15 minutes since the aluminum plate has a different contraction rate as compared to the support material. As the temperature of the build surface drops in the freezer, the printed part will then release itself from the build surface.

The printed sacrificial pattern has to be subjected to two stages of post-processing in order to remove all of the support material (i.e. wax). In the first stage, the printed part is kept in an oven at a temperature of 58^{o} C at which the wax support

material will melt away; the oven temperature should not exceed 60^{o}C as prolonged exposure to high temperature can lead to warping of the part. The duration of time the part must be kept in the oven varies based on its geometry; typically the time ranges from one hour to four hours (for small to larger structures respectively). Once all the wax appears to have drained out, the printed part will then be subjected to the second stage of post-processing, a lukewarm oil bath in an ultrasonic cleaner intended to remove any trace amounts of wax that remain on the printed part. Multiple cleaning cycles can be run on the printed part to ensure that all trace amounts of wax have been removed as these trace amounts of wax on the surface of the printed part will not be visible to the naked eye.

Upon completion of the post-processing, the first stage of the investment casting process known as the shell building process begins. In this stage, the printed sacrificial pattern is coated with a mixture of fused silica (Ranco-sil4) and binder this mixture is then further coated with a fine-grained stucco and coarse-grained stucco (Ranco-silA and Ranco-silB respectively, from suppliers Ransom & Randolph). The first four coats are composed of Ranco-silA with the following three coats being of Ranco-silB. The fine grained nature of Ranco-silA helps in achieving good surface finish on the final cast part whereas Ranco-silB provides additional strength to the ceramic shell. After application of each coat, the sacrificial pattern is allowed to dry for several hours before application of the next coat. The fully built and dried ceramic shell must then be placed in an oven at 80^{o}C to remove all moisture. This drying process is necessary because molten aluminum reacts violently with moisture. The binder used has a color indicator which appears to be bright yellow when wet but white when dry; this color change indicates

that the moisture is fully removed from the mold. The oven temperature is set to 80^{o}C to ensure gradual remove of moisture without the formation of steam, the presence of which is detrimental to the ceramic shell.

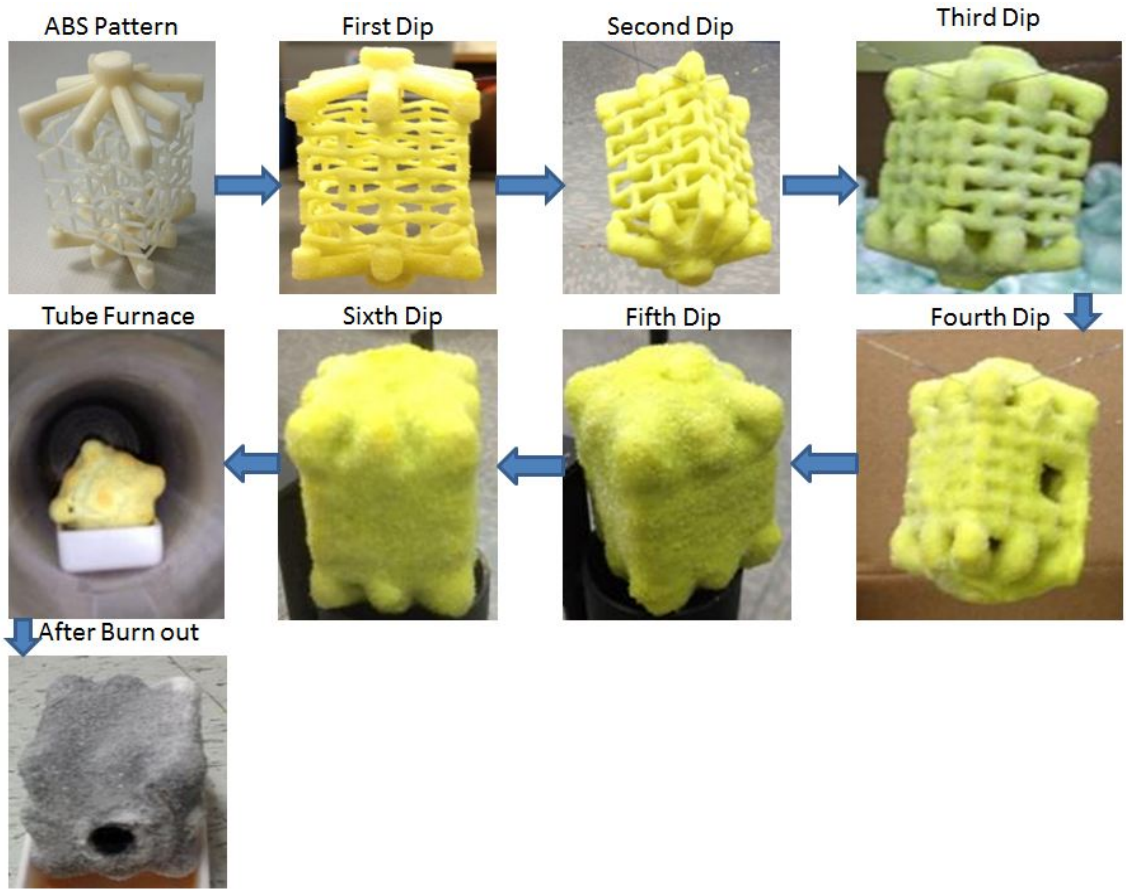

Figure 8: Shell Building Process

The sacrificial pattern which has been coated with ceramic material must be burned out to create a hollow cavity in the mold. The temperature required for the burn-out depends on the material of the sacrificial pattern used and the temperature profile required to burn out ABS and FC-720, the latter of which is a polypropylene like material [28] developed by Objet Geometries Ltd, are shown in figure 9.

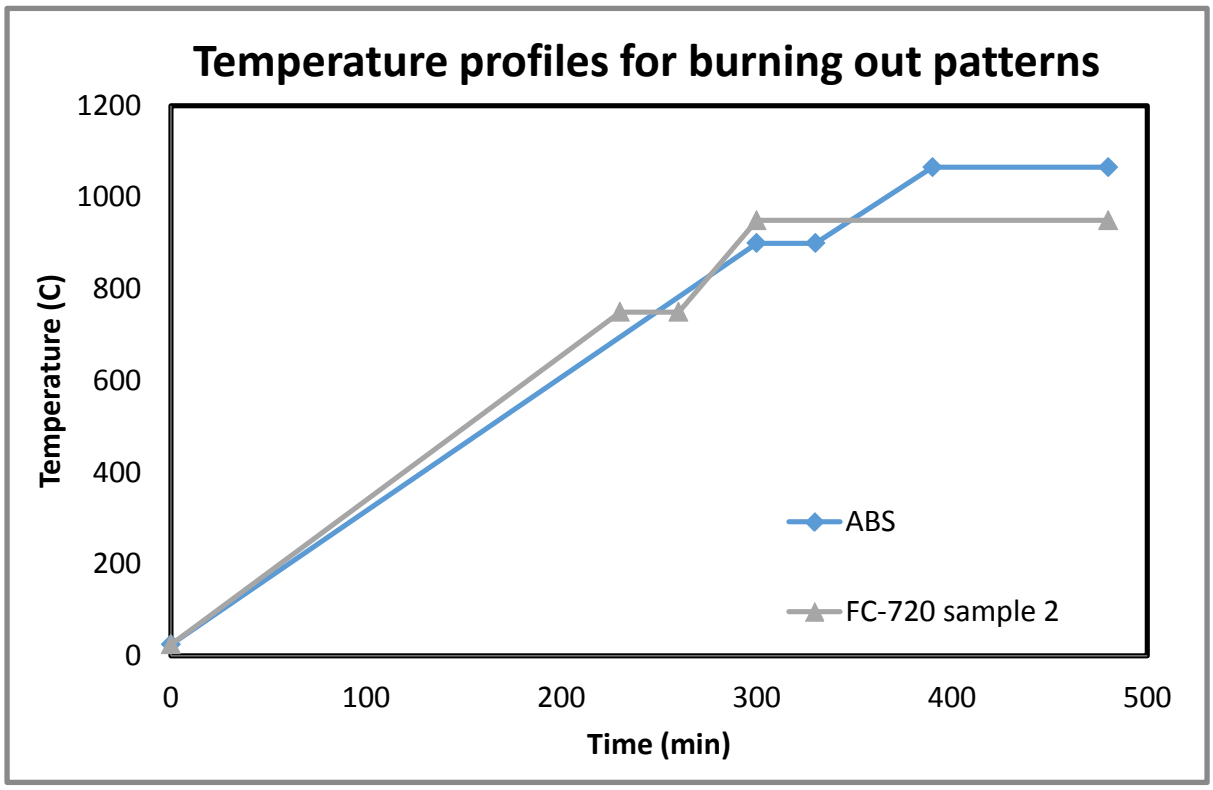

Figure 9: Temperature Profile

Thermal expansion of the pattern and the ceramic shell leads to generation of stresses and these stresses can cause cracks in the ceramic shell. If there exists a high difference in the values of the linear thermal expansion coefficient between the fused silica in the ceramic shell and the sacrificial pattern used, there will be shell cracking. Thermal stresses developed are discussed in Chapter 6.

(a) Inlet Top View

(b) Section View - Inlet & Gates

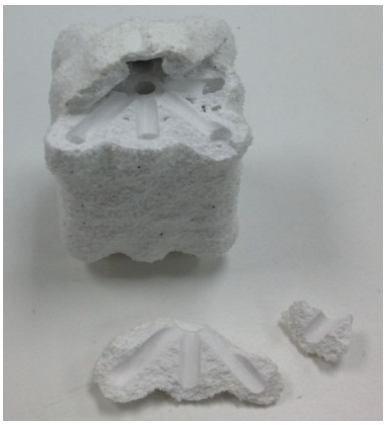

(c) Section View - Gates

(d) Section View – Midsection of Mold

Figure 10: Sectional View of the Inlet and Gating System.

In order to minimize casting defects in the final product, it is essential that the molten metal flows through the mold, thus pushing the air out; for this, there must be sufficient molten metal to flow through all channels.“The purpose of a runner system is to achieve a desired flow rate into specific locations of a casting cavity, smoothly and efficiently”[29].

The burn-out process involves subjecting the mold with the sacrificial pattern to elevated temperatures to burn out the sacrificial pattern inside; this results in the creation of a hollow mold cavity, which will be filled with molten metal. Sacrificial patterns of three different materials—ABS, Fullcure 720 and Procast—were used to build three separate molds. Each of these materials has a different burn-out temperature and linear thermal expansion coefficient.

Table 4: Sacrificial Pattern Properties [30] [31][32][33][34]

	ABS (FDM)	FC-720 (SLA)	VisiJetProcast	Wax
Density	1.05 g/cm^3	N/A	1.02 g/cm^3	0.88 - 0.92 g/cm3
Shrinkage	0.005 /in/in	N/A	N/A	N/A
Coefficient of thermal expansion	0.72*10^{-6}	0.0014 - 0.0027	N/A	307 * 10^{-6}
Elongation at break %	>10	15-25	12.3	2.8
Tensile Strength	34.5 MPa	60.2 MPa	32 Mpa	1.369 MPa
Modulus of Elasticity	2206 MPa	2869 MPa	1724 Mpa	18.28 Mpa
Melting Temperature	225-265^{o}C	N/A	N/A	60^{o}C
Burn out Temperature	1066^{o}C	950^{o}C	700^{o}C	300^{o}C
Ash Content, %	<0.01	<0.01	0.01	N/A

Fused silica, having a linear thermal expansion coefficient (LTEC) of 0.4*10^{-6} /^{o}C, is comparable to the LTEC of ABS, which is 0.72*10^{-6} /^{o}C; conversely, FC-720 has a LTEC the range of 0.0014 - 0.0027 /^{o}C, which is much higher as compared to fused silica. As a result of this thermal expansion coefficient mismatch, we encountered shell

cracking with FC-720 pattern whereas there was no damage to the ceramic shell with the use of the ABS sacrificial pattern. Shells which were damaged during the burn-out process can be seen below:

Figure 11: Shell Cracking

Shell cracking was not experienced with the ABS sacrificial pattern. The ABS mold is shown below:

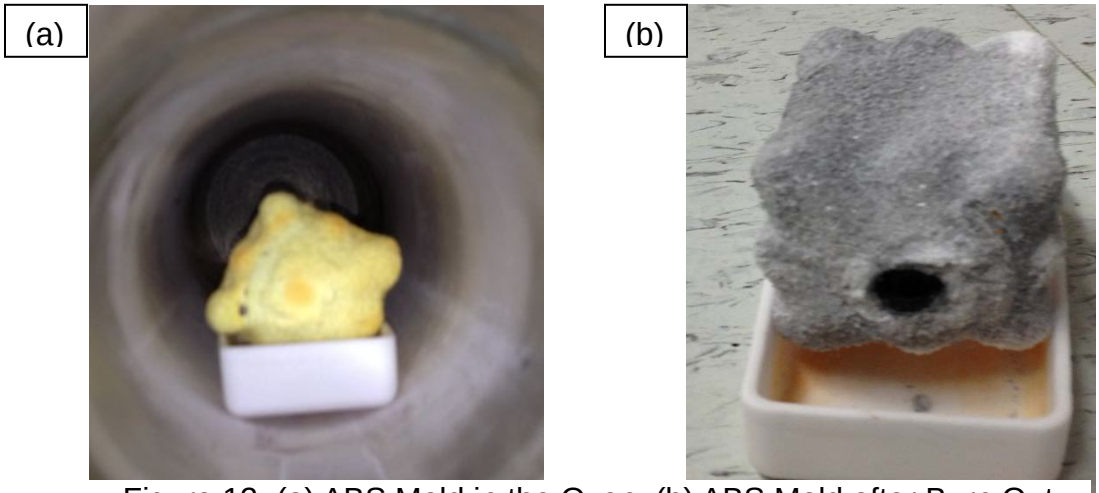

Figure 12: (a) ABS Mold in the Oven, (b) ABS Mold after Burn Out

Different approaches were carried out to fill the mold cavity with molten aluminum. The three different trials are explained below.

4.1 Trial 1 Molten Metal Filling

In this trial, a conventional metal casting process was used where the mold was placed in a sand bath to make sure it does not get disturbed, and the molten metal was hand poured into the mold cavity. On completing the pouring process, the shell was cracked open for inspection; upon doing so, it was noticed that there was pre-mature solidification of the molten metal at the very entrance of the gates. Results of this trial are shown in Chapter 6 of this document.

4.2 Trial 2 Molten Metal Filling

In an attempt to overcome the shortcomings of the first trial, certain changes were implemented to the metal filling process. The first change was to pre-heat the ceramic mold in order to reduce the temperature gradient between the ceramic mold and the molten metal. The second change was to immerse the ceramic shell into a pool of molten metal rather than pouring the molten metal from the top.

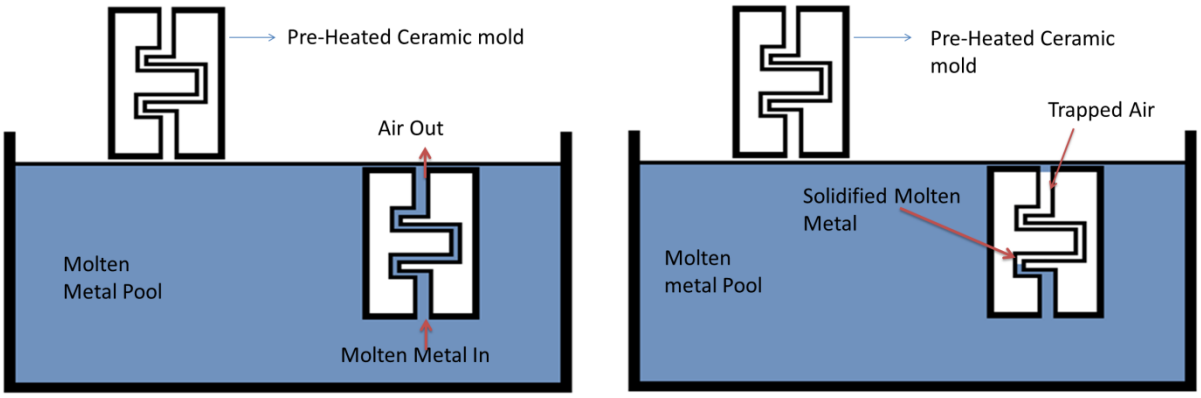

Figure 13: Trial 2 Hypothesis

The idea behind this hypothesis was to allow the molten metal to fill the mold cavity from the bottom-up and push the air out from the opening on the top surface. Though the desired results were not obtained, there was improved fluid flow seen with this method. The results of this trial are shown in Chapter 6 of this document.

4.3 Trial 3 Molten Metal Filling Using Suction Pump

Employing the same principle as in Trial 2, Trial 3 includes the addition of a suction pump to create a pressure drop within the mold cavity. The pressure gradient created between the surrounding atmosphere and the interiors of the hollow mold cavity will aid the flow of the molten metal through the channels of the mold cavity.

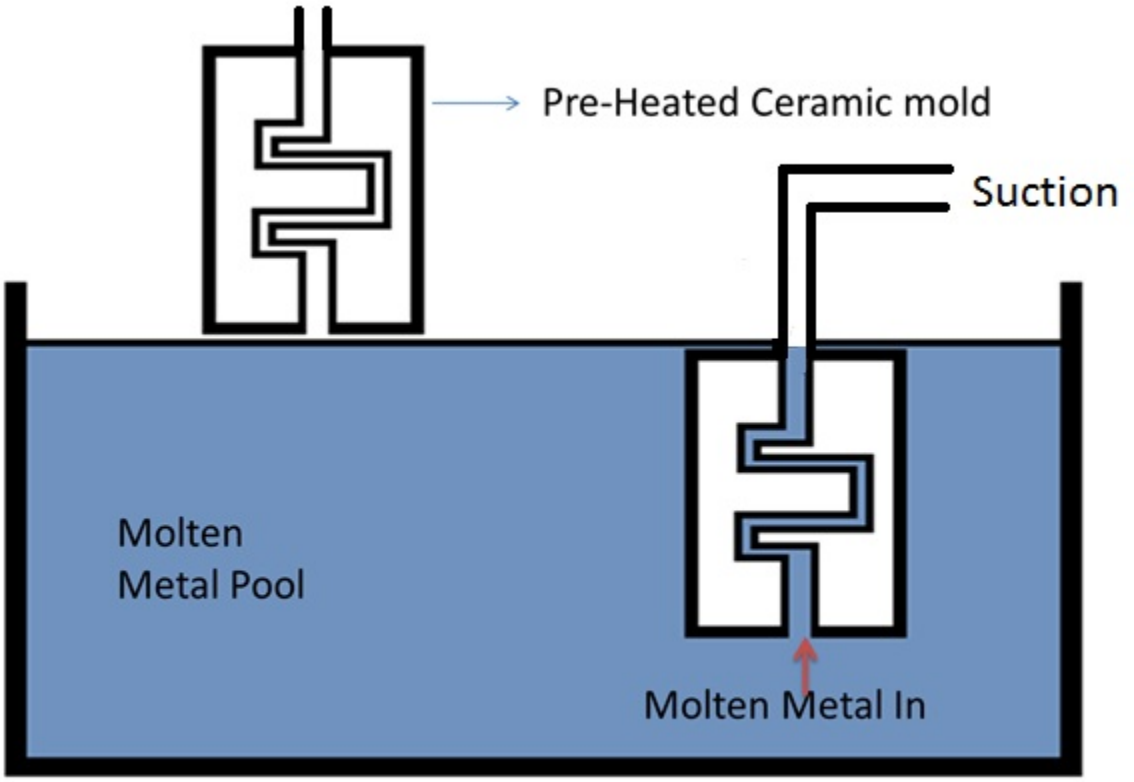

Figure 14: Trial 3 Hypothesis

To accommodate the suction pump, an additional change had to be made to the ceramic shell. A wax candle was used to provide a channel to connect to the suction pump, as illustrated in the following images:

(a)  (b) 

Figure 15: (a) ABS Sample with Wax Candle, (b) Sample with Ceramic Shell

CHAPTER 5

COST ANALYSIS

In this chapter, the process cost to manufacture metallic lattice structures by combining additive manufacturing and investment casting will be estimated. I will draw a comparison of the estimated cost of the AM-IC method with existing methods such as electron beam machining (EBM). We will also understand the major cost drivers in the additive manufacturing process and how these drivers influence the overall process cost. The manufacturing process includes the following stages:

1. Pre-processing of the job
2. Printing the job
3. Post-processing and cleaning the job
4. Shell building
5. Burn-out of sacrificial pattern
6. Molten metal filling

The major cost drivers are equipment cost, power consumption, material cost, and build cost. The build cost depends on several other factors such as labor cost and machine hourly rate [8]. The power consumption for the AM-IC process will include the power consumption of all of the auxiliary devices that are used. The power consumption cost of the auxiliary devices used in the AM-IC process for building 20 parts a year is

$$Power\ (W) = Voltage\ (V) * Current\ (A)$$

$$Power = 120 * 15$$

$$Power = 1800\ W$$

$$Cost = \frac{1800 * 9.6\ \left(\frac{hrs}{day}\right) * 20\ \left(\frac{days}{year}\right)}{1000}$$

$$Cost = 345.6\ \left(\frac{Kwh}{yr}\right) * 10\ (\frac{¢}{KWh})$$

$$Cost = 34.56\ \$/yr$$

$$Cost = 1056\ \left(\frac{Kwh}{yr}\right) * 10\ (\frac{¢}{KWh})$$

$$Cost = 105.6\ \$/yr$$

Power consumption cost of EBM

$$Power\ (W) = Voltage\ (V) * Current\ (A)$$

$$Power = 1200 * 32$$

$$Power 384000\ W$$

$$Cost = \frac{38400 * 4\ \left(\frac{hrs}{day}\right) * 20\ \left(\frac{days}{year}\right)}{1000}$$

$$Cost = 3072\ \left(\frac{Kwh}{yr}\right) * 10\ (\frac{¢}{KWh})$$

$$Cost = 307.2\ \$/yr$$

Mixer for slurry

$$Power\ (W) = Voltage\ (V) * Current\ (A)$$

$$Power = 115 * 2$$

$$Power = 230\ W$$

$$Cost = \frac{230 * 24\ \left(\frac{hrs}{day}\right) * 60\ \left(\frac{days}{year}\right)}{1000}$$

$$Cost = 331.2\ \left(\frac{Kwh}{yr}\right) * 10\ (\frac{¢}{KWh})$$

$$Cost = 33.12\ \$/yr$$

Post-processing oven

$$Power\ (W) = Voltage\ (V) * Current\ (A)$$

$$Power = 120 * 10$$

$$Power = 1200\ W$$

$$Cost = \frac{1200 * 4\ \left(\frac{hrs}{day}\right) * 20\ \left(\frac{days}{year}\right)}{1000}$$

$$Cost = 96\ \left(\frac{Kwh}{yr}\right) * 10\ (\frac{¢}{KWh})$$

$$Cost = 9.6\ \$/yr$$

Tube furnace

$$Power\ (W) = Voltage\ (V) * Current\ (A)$$

$$Power = 220 * 30$$

$$Power = 6600\ W$$

$$Cost = \frac{6600 * 8\ \left(\frac{hrs}{day}\right) * 20\ \left(\frac{days}{year}\right)}{1000}$$

$$Cost = 105.6\ \$/yr$$

A comparison of different cost drivers between manufacturing lattice structures from electron beam machining and from additive manufacturing combined with investment casting can be seen in the figures below.

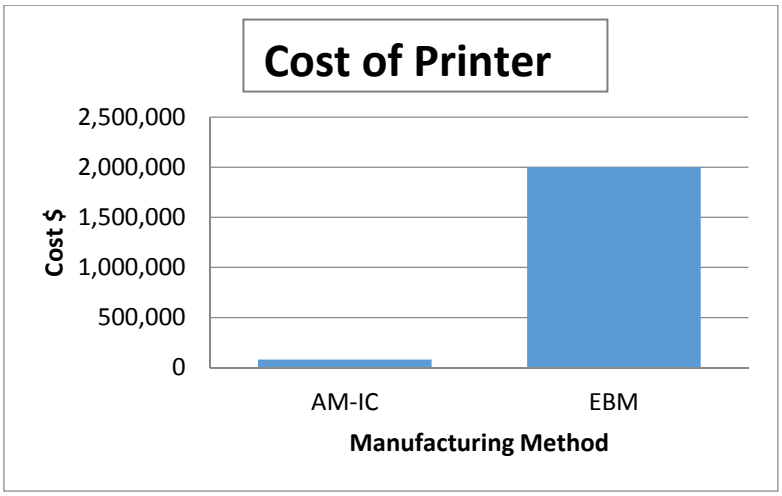

Figure 17: Comparison of Printer Cost

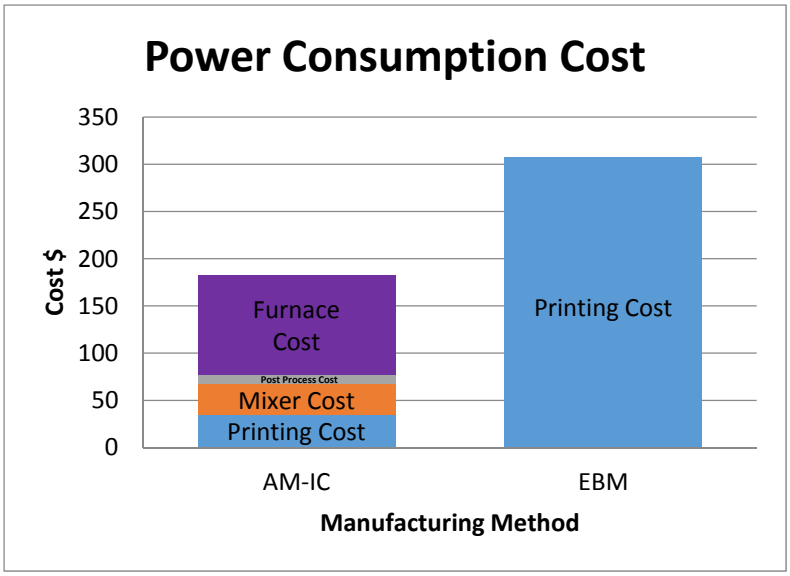

Figure 16: Comparison of Power Consumption

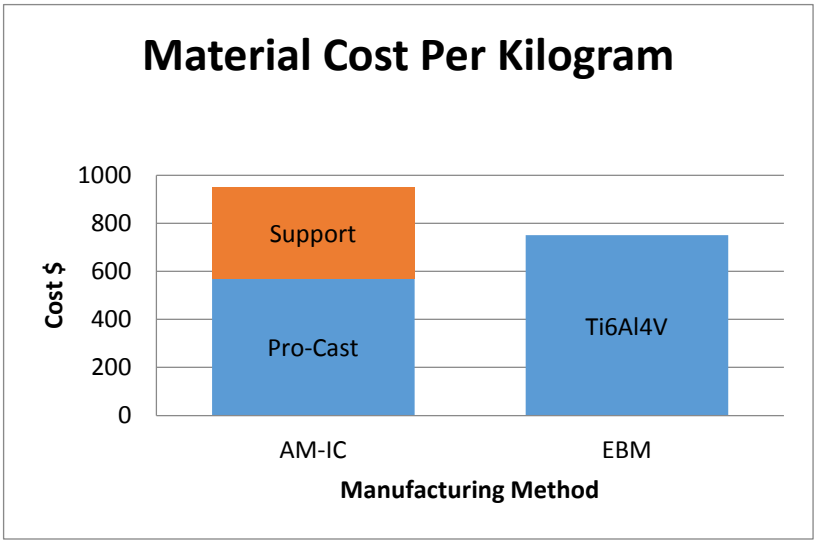

Figure 18: Comparison of Material Cost

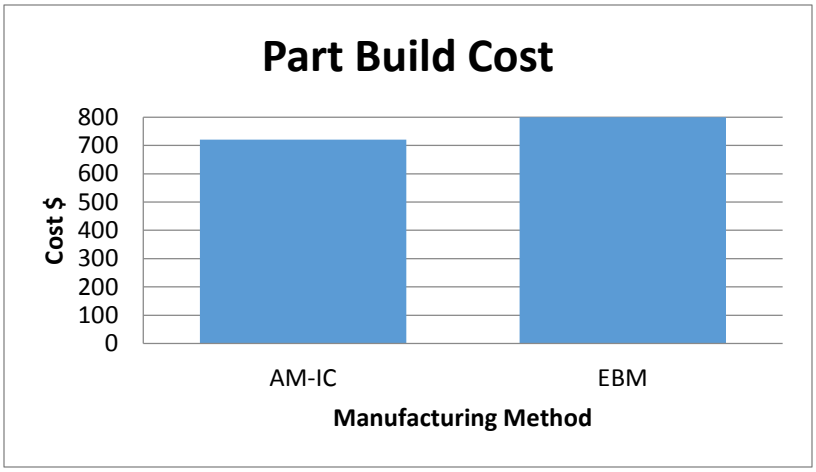

Figure 19: Comparison of Part Build Cost

The total cost of the AM-IC process is inexpensive as compared to the electron beam machining (EBM) because of the tremendous difference in the initial investment cost of the 3D-printing machine. The total cost comparison is shown in the graph below, and it can be clearly seen that the difference in initial investment is the key factor of the overall cost difference.

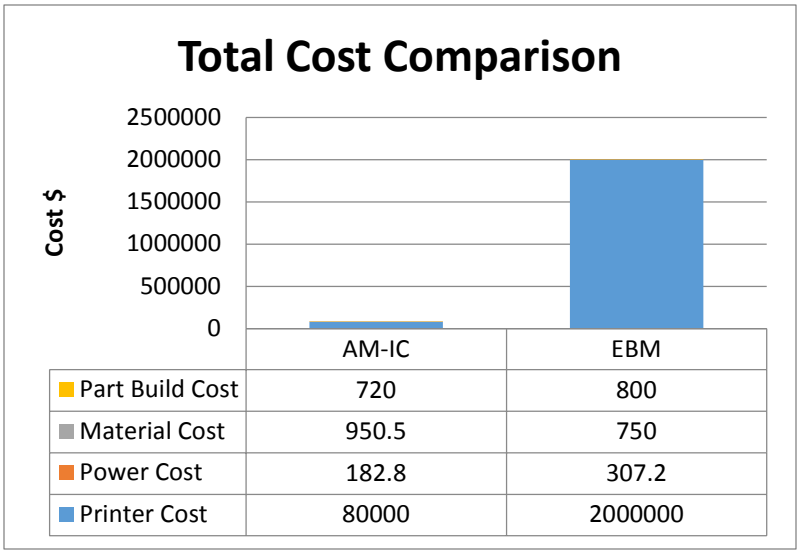

	AM-IC	EBM
Part Build Cost	720	800
Material Cost	950.5	750
Power Cost	182.8	307.2
Printer Cost	80000	2000000

Figure 20: Total Cost Comparison

CHAPTER 6

RESULTS AND ANALYSIS

6.1 Trial 1 Results

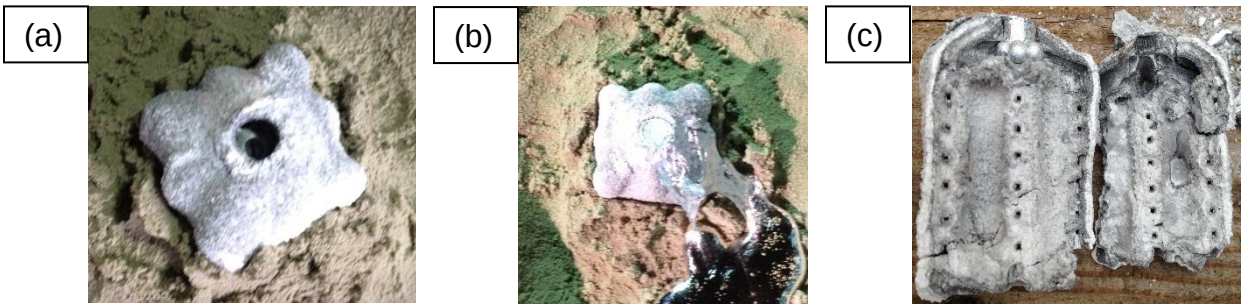

Figure 21: Trial 1 (a) Mold Placed in Sand Bath, (b) Poured Molten Metal (c) Pre-Mature Solidification

On trying to understand the nature of pre-mature solidification of the molten metal at the entrance of the gates, we concluded the primary factor to be the temperature gradient between the molten metal (approximately 660^{o}C) and the ceramic mold, which is at room temperature. As a result of this vast temperature gradient, the temperature of the molten aluminum drops drastically when it comes in contact with the ceramic shell walls. By nature, molten aluminum resists flow, becoming a sluggish liquid as its temperature drops. Eventually, the cooling aluminum becomes increasingly viscous until flow stops completely; as a result, the solidification of the aluminum is as observed in figure 21.

6.2 Trial 2 Results

(a) (b) (c)

Figure 22: Trial 2 (a) Pre-Heat Mold, (b) Mold Dipped in Molten Metal Pool (c) Opened Shell

On inspecting the shell after the dipping process, it was observed that the molten metal did undergo pre-mature solidification after it passed through the gates; however, a noticeable improvement in fluid flow was achieved.

Figure 23: Solidified Metal Removed from Cast

It can be seen from the above image that molten metal solidified after entering the narrow 1mm diameter channels; this is an improvement in flow from the first trial. This improvement in molten metal flow through the mold cavity is in agreement with the velocity profile obtained from the analytical approach. In this approach, the velocity of the molten metal increases with an increase in temperature above the melting point of the metal while maintaining the shell temperature above the melting point of the fluid.

6.3 Trial 3 Results

Molten metal filling using the suction method could not be carried out as there were failures encountered during the sacrificial burn-out process.

Formation of Tar

The sacrificial pattern used was ABS. For the complete burnout of the pattern, it was exposed to a maximum temperature of 1066^{o}C[16].The corresponding temperature cycle is shown in the following graph:

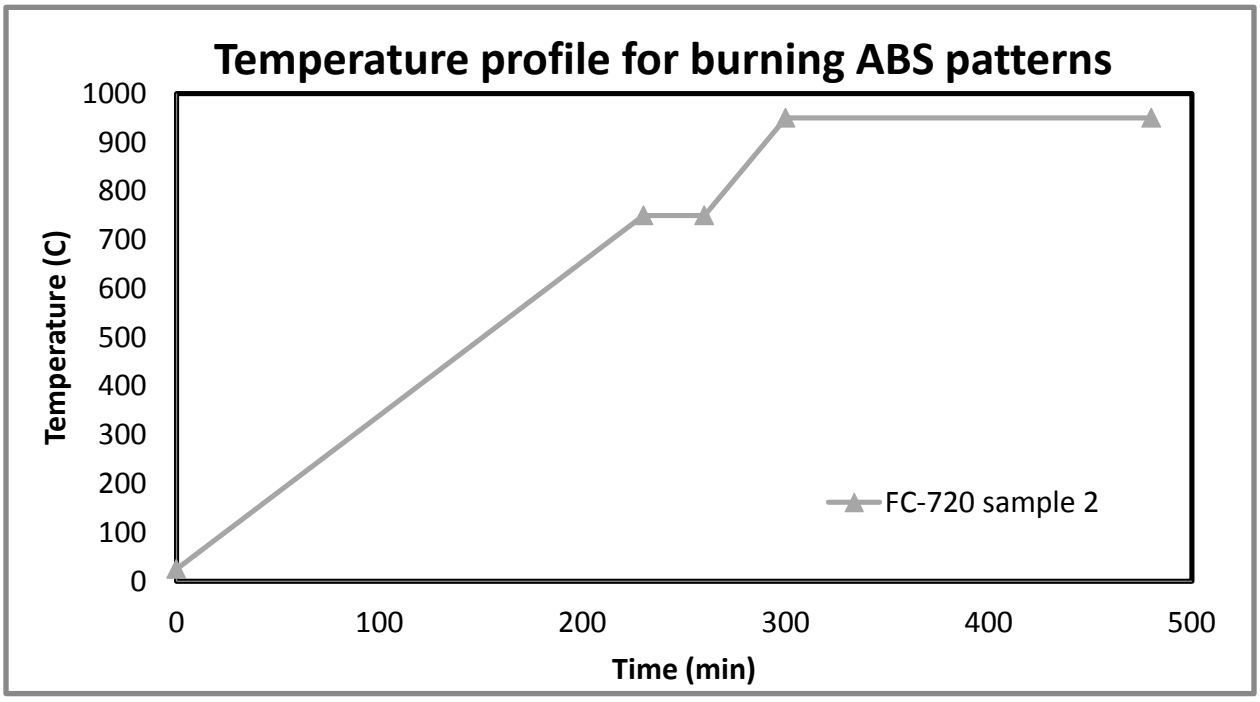

Figure 24: Burn out Temperature Profile

pump, has an auto-ignition temperature at 245^{o}C [35]. The mold in this study was placed in a tube furnace and exposed to a gradual temperature rise of 5^{o}C per minute up to 200^{o}C and then 2^{o}C per minute until it reached the target temperature of 1066^{o}C. Previous studies have demonstrated that the exposure of wax to temperature increase results in melting beginning at 60^{o}C, vaporization at 238^{o}C and finally, auto-ignition at 245^{o}C. As a result of these findings, it may be that our mold and corresponding wax underwent a similar transformation.

Since the furnace is an enclosed space, the fumes accumulate around the ceramic shell and ignite; the resulting flame engulfs the ceramic shell andleads to formation of a sticky, tar-like substance within the shell walls that coagulates and blocks the hollow cavity inside. Eventually, this results in the obstruction of flow of molten metals.

Although the ABS pattern does burnout well before the target temperature of 1066^{o}C, this abrupt burn out leaves behind residual matter in the narrow mold cavity.

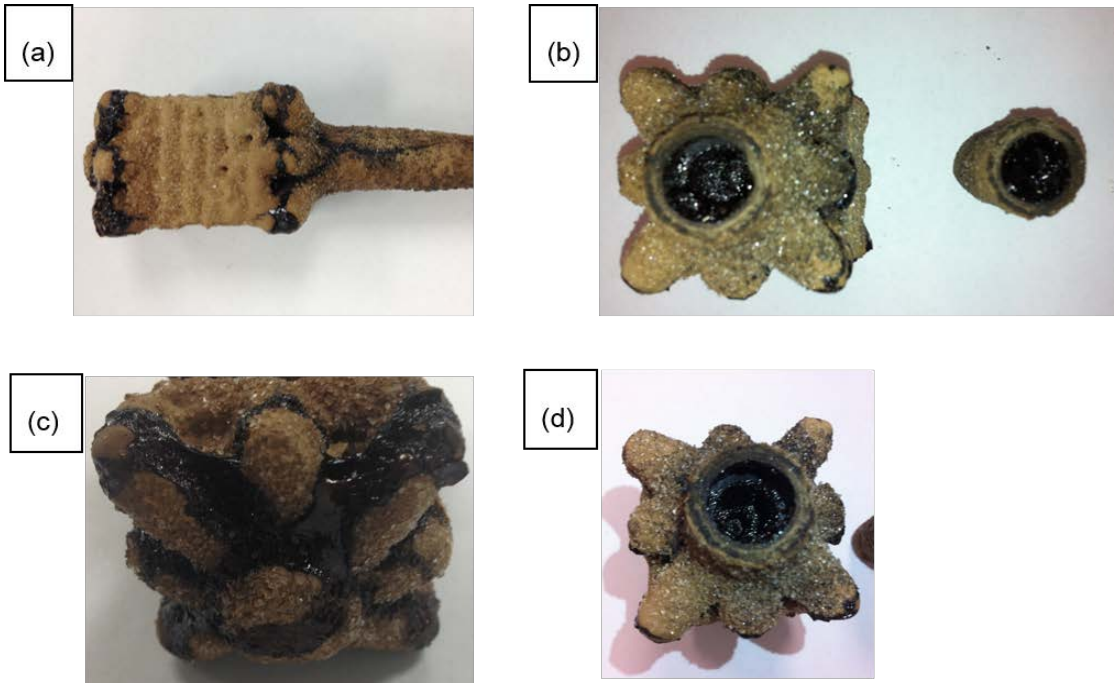

Figure 25: Tar Deposit on Shell Surface.

Upon examining the ceramic shell after the burn out process, there were noticeable surface cracks all over the ceramic shell body; the surface cracks will be analyzed according to the material of the sacrificial pattern used.

CHAPTER 7

FAILURE ANALYSIS OF CERAMIC SHELL: DETERMINATION OF MELTING POINT AND THERMAL STRESS ANALYSIS

To determine the melting point of the sacrificial pattern material, a differential scanning calorimeter is used. In a typical differential scanning calorimetry (DSC) experiment, the difference in power required to heat a reference pan and sample pan is monitored as a function of temperature at a fixed temperature sweep rate. This procedure allows for the examination of both exothermic and endothermic events and the determination of their heats. Typically, DSC sample pans are made of aluminum, but gold, platinum, and stainless steel have been used for specific applications requiring higher temperatures or pressures [36].

The DSC that was used in our experiments is the DSC 6 PerkinElmer which runs on the Pyris series software. The samples tested are wax, Pro-Cast, FC-720 and ABS. These samples were prepared in aluminum pans (30 µL), weighed, and crimped. A blank aluminum reference pan is also prepared and placed in the DSC along with the pan carrying the material sample; nitrogen gas (20 ml/min) is used, which is maintained at a pressure between 50-60 psi. For wax, the test cycle is as follows:

- Hold for 2 minutes at 30^{o}C.
- Heat from 30^{o}C to 100^{o}C at 10^{o}C/min.
- Hold 5 minutes at 100^{o}C.
- Cool from 100^{o}C to 30^{o}C at 10^{o}C/min.

For Pro-Cast, FC-720 and ABS a similar test cycle is employed but with elevated temperatures:

- Hold for 2 minutes at 50^{o}C.
- Heat from 50^{o}C to 400^{o}C at 10^{o}C/min.
- Hold 5 minutes at 400^{o}C.
- Cool from 100^{o}C to 50^{o}C at 10^{o}C/min.

Shown below are the results of the DSC test to determine the glass transition temperature (T_g) and melting temperature (T_m):

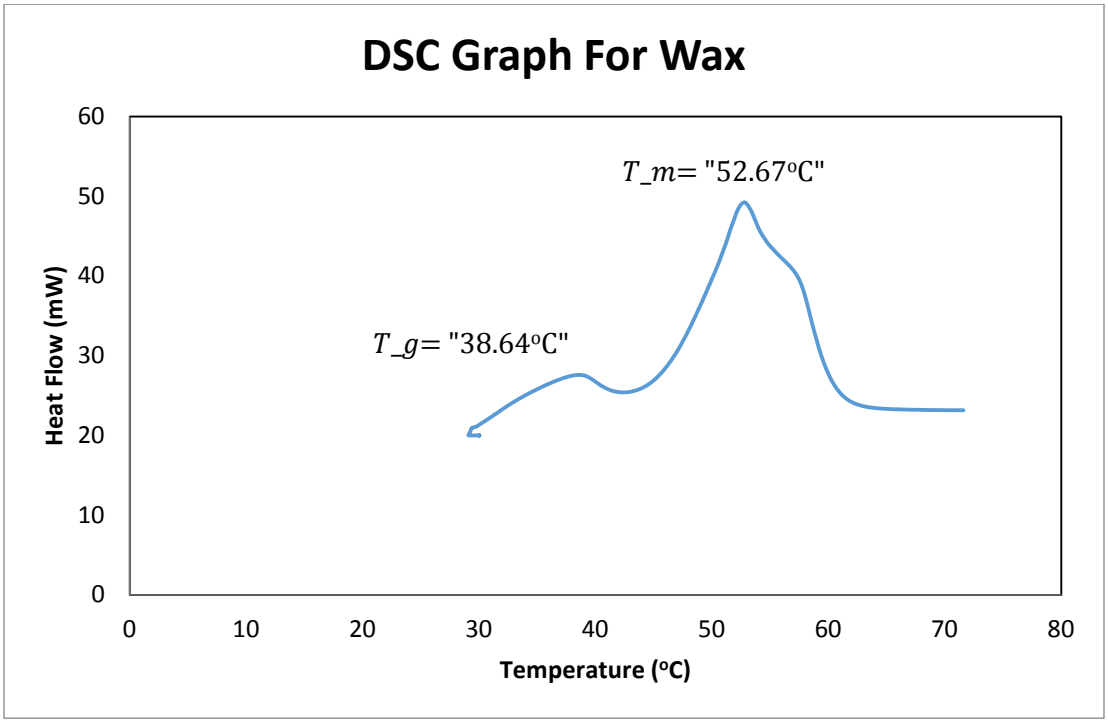

Figure 26 : DSC Graph for Wax

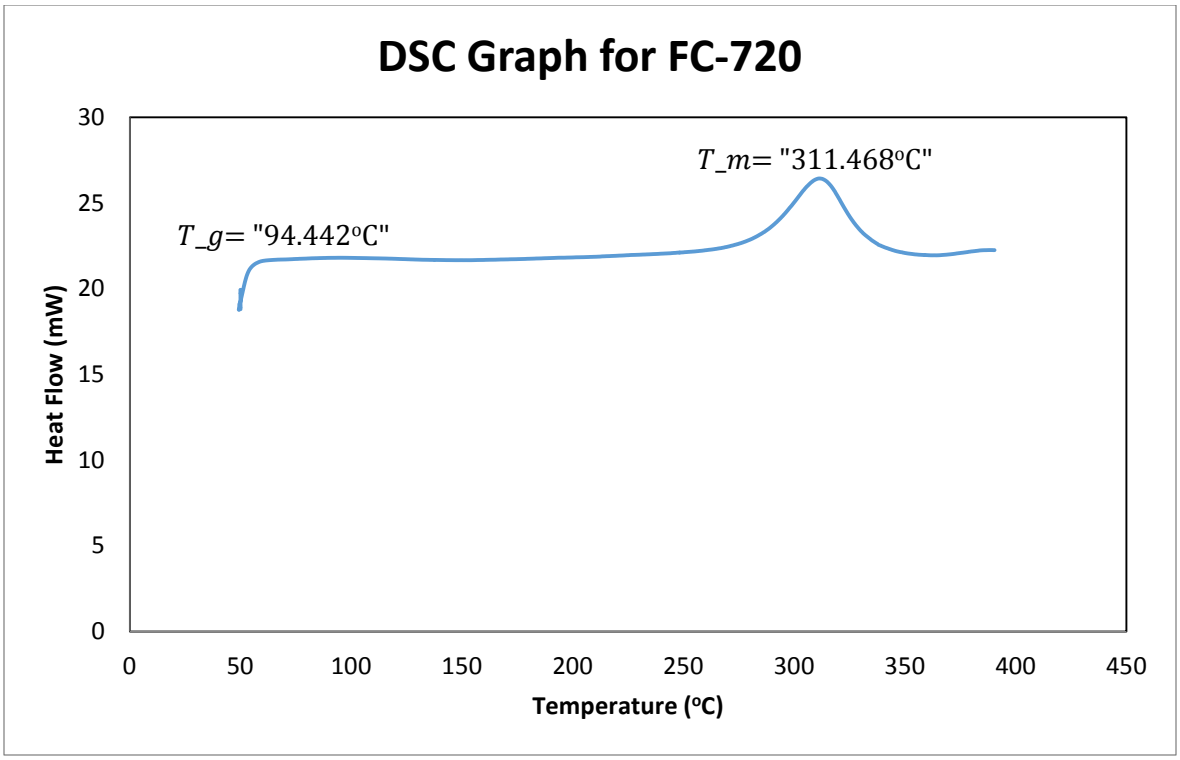

Figure 27 : DSC Graph for FC-720

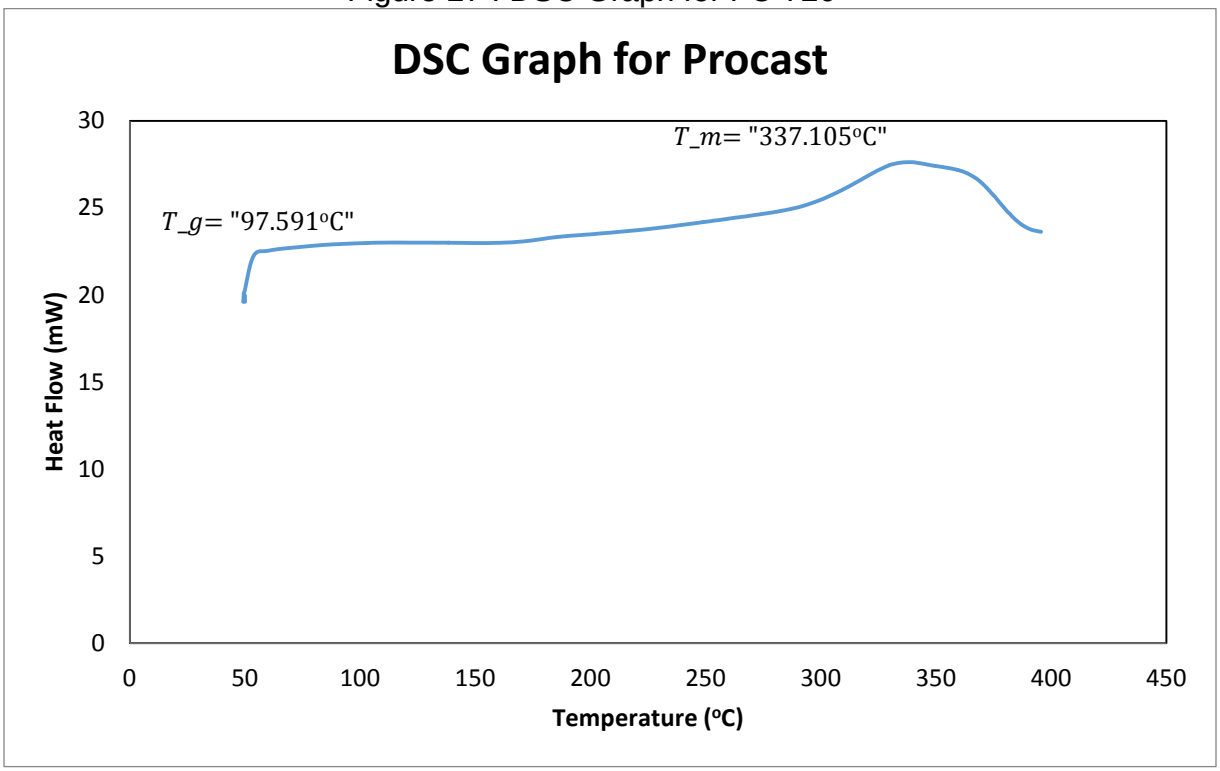

Figure 28 : DSC Graph for Pro-Cast

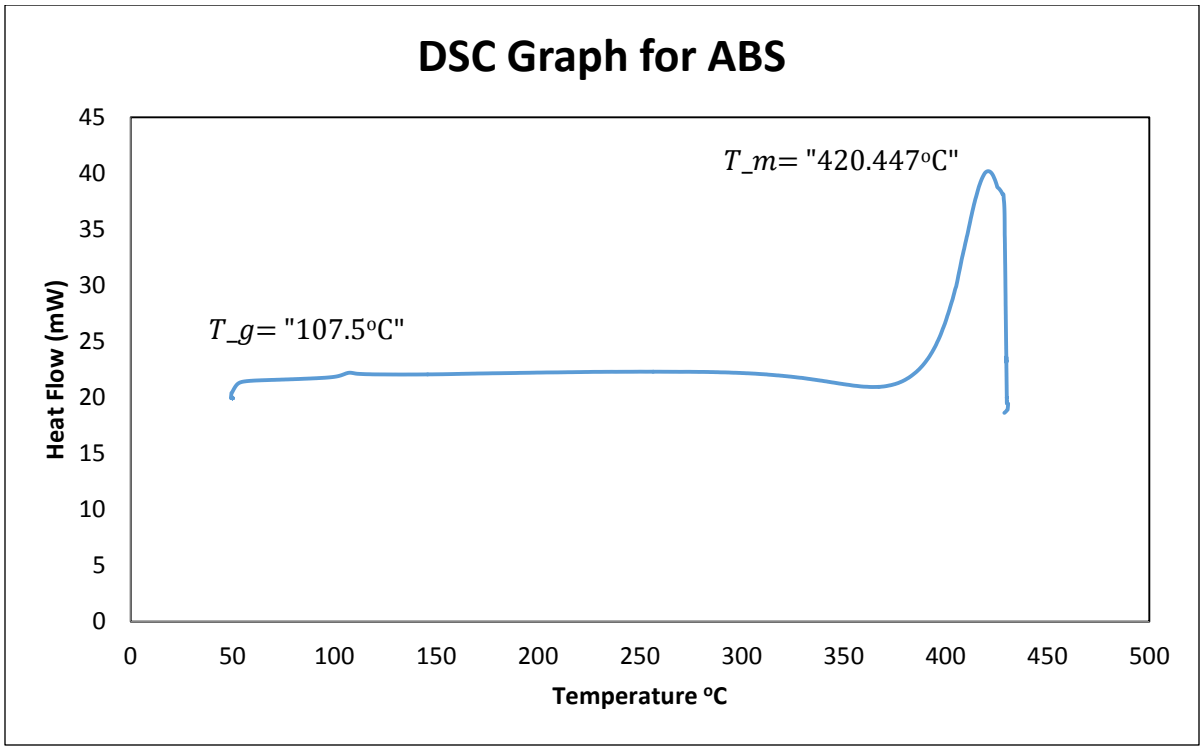

Figure 29 : DSC Graph for ABS

Table 5: Glass Transition and Melting Temperature for Samples

Material	Sample weight (mg)	T_g (^oC)	T_m (^oC)
Wax	9.41	38.64	52.67
FC-720	7.65	94.44	311.47
Pro-cast	10.25	97.59	337.10
ABS	11.1	107.5	420.45

In order to calculate the thermal stresses developed, we used the stress-strain relationship for an isotropic material in the spherical coordinate system[37].Thermal stresses are generated at the boundary where material 1(sacrificial pattern) meets material 2 (ceramic shell) as a result of thermal expansion mismatch between the two

materials. Using cylindrical coordinates, any point on a feature will have specific(r, θ, z) coordinates. The radial direction is represented by r, tangential direction is represented by θ, and axial direction by z. The stresses acting on a small element of material in the cylindrical coordinate system are shown in figure 28.

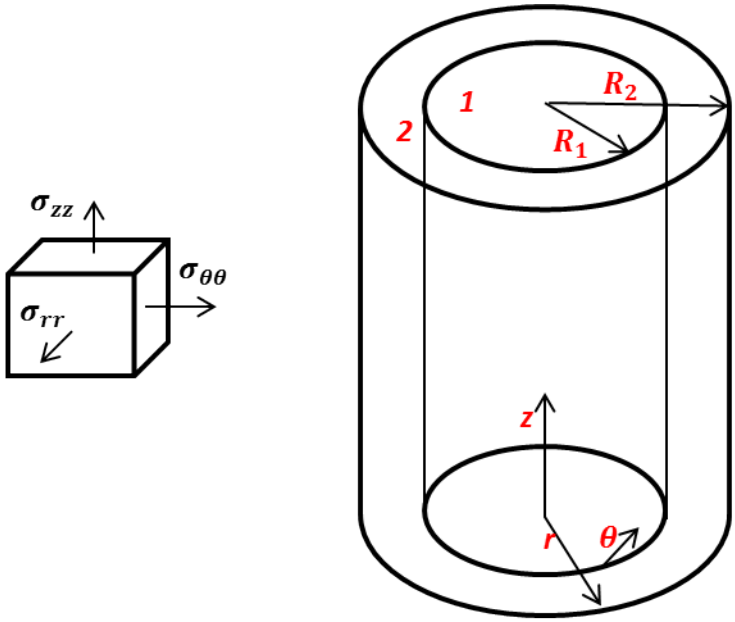

Figure 30 : Cylindrical Representation of Pattern and Ceramic Shell

The normal strainsε_{rr},$\varepsilon_{\theta\theta}$, and ε_{zz} are a measure of the elongation/shortening of the material per unit length, in the radial, tangential, and axial direction. The shear strains$2\varepsilon_{\theta z}$,$2\varepsilon_{rz}$, and $2\varepsilon_{r\theta}$ represent the change in right angles between the elements along the coordinate system. The stress-strain relationship is shown below, where E is the Youngs modulus of the material, υ is the poisons ratio, and α is the linear thermal coefficient of expansion.

$$\begin{bmatrix} \varepsilon_{rr} \\ \varepsilon_{\theta\theta} \\ \varepsilon_{zz} \\ 2\varepsilon_{\theta z} \\ 2\varepsilon_{rz} \\ 2\varepsilon_{r\theta} \end{bmatrix} = \left[\frac{1}{E}\right] \begin{bmatrix} 1 & -\upsilon & -\upsilon & 0 & 0 & 0 \\ -\upsilon & 1 & -\upsilon & 0 & 0 & 0 \\ -\upsilon & -\upsilon & 1 & 0 & 0 & 0 \\ 0 & 0 & 0 & 2(1+\upsilon) & 0 & 0 \\ 0 & 0 & 0 & 0 & 2(1+\upsilon) & 0 \\ 0 & 0 & 0 & 0 & 0 & 2(1+\upsilon) \end{bmatrix} \begin{bmatrix} \sigma_{rr} \\ \sigma_{\theta\theta} \\ \sigma_{zz} \\ \sigma_{\theta z} \\ \sigma_{rz} \\ \sigma_{r\theta} \end{bmatrix} + (\alpha\Delta T) \begin{bmatrix} 1 \\ 1 \\ 1 \\ 0 \\ 0 \\ 0 \end{bmatrix}$$

Since there is no external force present, the above equation reduces to

$$\begin{bmatrix} \varepsilon_{rr} \\ \varepsilon_{\theta\theta} \\ \varepsilon_{zz} \\ 2\varepsilon_{\theta z} \\ 2\varepsilon_{rz} \\ 2\varepsilon_{r\theta} \end{bmatrix} = [0] + (\alpha\Delta T) \begin{bmatrix} 1 \\ 1 \\ 1 \\ 0 \\ 0 \\ 0 \end{bmatrix}$$

It can be seen that the shear strain term does not exist, and only principle strains will be developed due to the thermal load. The thermal stresses can be calculated using the following relationship:

$$\begin{bmatrix} \sigma_{rr} \\ \sigma_{\theta\theta} \\ \sigma_{zz} \\ \sigma_{\theta z} \\ \sigma_{rz} \\ \sigma_{r\theta} \end{bmatrix}_{Thermal} = E \begin{bmatrix} \varepsilon_{rr} \\ \varepsilon_{\theta\theta} \\ \varepsilon_{zz} \\ 2\varepsilon_{\theta z} \\ 2\varepsilon_{rz} \\ 2\varepsilon_{r\theta} \end{bmatrix}_{Thermal}$$

Fullcure-720 with fused silica shell, material properties are taken from table 2 of this document:

$$\alpha_{FC-720} = 0.0020\ /C^o$$

$$\varepsilon_{rr} = \alpha_{FC-720} * \Delta T$$

$$\varepsilon_{rr} = \alpha_{FC-720} * (T_m - T_{amb})$$

$T_m$is the melting temperature of the pattern material and $T_{amb}$is the ambient temperature, both in degree Celsius.

$$\varepsilon_{rr} = 0.0020 * (311.46 - 25)$$

$$\varepsilon_{rr} = 0.57 = \varepsilon_{\theta\theta} = \varepsilon_{zz}$$

The principal stresses are

$$\sigma_{rr} = \varepsilon_{rr} * E_{FC-720}$$

$$\sigma_{rr} = 0.57 * 2869\, MPa$$

$$\sigma_{rr} = 1643.MPa = \sigma_{\theta\theta} = \sigma_{zz}$$

The maximum tensile stress of the fused silica shell is 50 MPa (σ_t).Using the principal stress failure criteria where the principal stressσ_{rr} should be less than or equal to maximum tensile stressσ_t, it can be seen that since$\sigma_{rr} \geq \sigma_t$there is a consequent failure of the ceramic shell. Acrylonitrile butadiene styrene (ABS) with fused silica shell,

$$\alpha_{ABS} = 0.72 * 10^{-6}\, /C^o$$

$$\varepsilon_{rr} = \alpha_{ABS} * \Delta T$$

$$\varepsilon_{rr} = \alpha_{ABS} * (T_m - T_{amb})$$

$$\varepsilon_{rr} = 0.72 * 10^{-6} * (395.5)$$

$$\varepsilon_{rr} = 2.8 * 10^{-4} = \varepsilon_{\theta\theta} = \varepsilon_{zz}$$

The principal stresses are

$$\sigma_{rr} = \varepsilon_{rr} * E_{ABS}$$

$$\sigma_{rr} = 7.49 * 10^{-4} * 2206\, MPa$$

$$\sigma_{rr} = 0.62\, MPa = \sigma_{\theta\theta} = \sigma_{zz}$$

The maximum tensile stress of the fused silica shell is 50 MPa (σ_t).Using the principal stress failure criteria where the principal stress should be less than or equal to maximum tensile strength, it can be seen that$\sigma_{rr} \leq \sigma_t$, hence the ceramic shell is safe.

For wax with a fused silica shell,

$$\alpha_{Wax} = 307 * 10^{-6}\, /C^o$$

$$\varepsilon_{rr} = \alpha_{Wax} * \Delta T$$

$$\varepsilon_{rr} = \alpha_{Wax} * (T_m - T_{amb})$$

$$\varepsilon_{rr} = 307 * 10^{-6} * (27.67)$$

$$\varepsilon_{rr} = 8.49 * 10^{-3} = \varepsilon_{\theta\theta} = \varepsilon_{zz}$$

The principal stresses are

$$\sigma_{rr} = \varepsilon_{rr} * E_{Wax}$$

$$\sigma_{rr} = 8.49 * 10^{-3} * 18.28\, MPa$$

$$\sigma_{rr} = 0.155\, MPa = \sigma_{\theta\theta} = \sigma_{zz}$$

The maximum tensile stress of the fused silica shell is 50 MPa (σ_t).Using the principal stress failure criteria where the principal stressσ_{rr} should be less than or equal to maximum tensile stressσ_t, it can be seen that$\sigma_{rr} \leq \sigma_t$demonstrates that the ceramic shell will not undergo failure due the thermal stresses. However, cracks were noticed on the ceramic shell and can be attributed to the abnormal burn-out process that the mold was subjected to because the mold caught fire (i.e. thermal shock) inside the high-temperature furnace.

Figure 31: Shell Cracks.

CHAPTER 8

CONCLUSION AND FUTURE WORK

8.1 Conclusion

Additive manufacturing is a relatively new process introduced less than a decade ago. In this thesis, additive manufacturing was combined with investment casting. Sacrificial patterns of different materials developed from various additive manufacturing techniques were used. Glass transition temperature and melting temperature of the sacrificial patterns were characterized to understand the behavior of the materials when exposed to high temperatures during the burn-out process. Thermal stress analysis that was carried out to study the ceramic shell cracking indicates that acrylonitrile butadiene styrene (ABS)and wax are well suited to be used as a sacrificial pattern. Experimentation also highlighted the defects and problems that were encountered during the manufacturing process; however, changes were employed based on our experimental hypothesis. Results of the analytical approach clearly indicate that there is an increase in the flow velocity by increasing the temperature of the molten metal pool beyond its melting point. Incorporating the hypothesis and the findings of the analytical study led to improved results as shown in figure 24.Results of the cost analysis clearly indicate that additive manufacturing combined with investment casting is 20 times more inexpensive, demonstrating economic viability as compared to electron beam machining. As a result of these findings, further research must be carried out to reduce the casting defects since the combined AM-IC process will greatly reduce the cost associated with fabricating cellular metals.

8.2 Future Work

One of the reasons that the fabrication process could not be carried out in the third trial was due to the shell cracking. This problem could be overcome by using a sacrificial pattern with a comparable linear thermal coefficient of expansion and an appropriate furnace to vent the fumes that are generated during the burn-out process. Furthermore, by venting these fumes, auto ignition will not take place, and the sacrificial pattern will be able to undergo complete burnout without damage to the ceramic shell and formation of the aforementioned tar-like substance. Secondly, poor fluidity was observed throughout the study; consequently, an experimental test rig will be setup to accommodate a suction pump, which will provide an additional driving force for the liquid to flow through the narrow channels of the hollow mold cavity. These changes are expected to show further reduction in casting defects.

BIBLIOGRAPHY

[1]. Bidwell, H. T. Investment Casting. s.l. : The machinery publishing CO., LTD., 1969.

[2]. Kalpakjian, Serope and Schmid, Steven R. Manufacturing Processes for Engineering Materials: Pearson, 2009.

[3]. Ian, Gibson, David, Rosen W and Brent, Stucker. Additive Manufacturing Technologies. New York : Springer, 2010.

[4]. An examination of the alternative methods used by the investment casting industry to produce sacrificial patterns. Winter, Jr, Daniel T. Florida : s.n., 2009. IMECE.

[5]. Mechanical Evaluation of Porous (Ti6Al4V) Structures with Electron Beam Melting (EBM). Parathasarathy , Jayanthi, et al. Norman : Elsevier, 2010.

[6]. Larsson, Morgan, Lindhe, Ulf and Harrysson, Ola. Rapid Manufactuing with Electron Beam Melting (EBM) -A Manufacturing Revolution?

[7]. Rapid Prototyping: Principles and Applications. Chee Kai Chua, Kah Fai Leong: World Scientific, 2003. ISBN-981-238-711-1.

[8]. Analyzing Product Lifecycle Costs for a Better Understanding of Cost Drivers in Additive Manufacturing. Lindemann, C, et al 2012.

[9]. Design for additive manufacturing. Vayre, B, Vignat, F and Villeneuve, F. 2012, Elsevier.

[10]. A Comparison of case-based reasoning and regression analysis. Banga, Karan and Takai, Shun. Montreal : ASME, 2010. ASME 2010 International Design Engineering Technical Conferences & Computers and Information in Engineering Conference.

[11]. Incorporating cost and resource efficiency into the development of green cycling technologies. Yang, Q Z, Qi, G J and Low, H C. Montreal : s.n., 2010. ASME.

[12]. Metal Fabrication by Additive Manufacturing Using Laser and Electron Beam Melting Technologies. Murr, Lawrence E, et al., et al. El Paso : Elsevier, 2012.

[13]. Cellular metals manufacturing. Wadley, N G Wadley. 2002, Advanced research materials.

[14]. The structural performance of near-optimized truss core panels. chiras, S, et al., et al. 2002, International Journal of Solids and Structures. 56

[15]. Lattice truss structures from expanded metal sheet. Kooistra, Gregory W and Wadley, Haydn N G. 2005, Material and Design.
[16]. Fabrication and structural performance of periodic cellular metal sandwich structures. Wadley, Haydn N G, Fleck, Norman A and Evans, Anthony G. s.l. : Elsevier, 2003, Composites and science Technology.
[17]. Manufacture, Characterization and application of cellular metals and metal foams. Banhart, John. 2001, Progress in Materials Science.
[18]. Modeling of Metal Delivery to Continuous Casting Moulds. Herbertson, J, et al., et al. Warrendale : ISS, 1991, Vol. 74.
[19]. Comparison of Four Methods to evaluate Fluid Velocities in a Continuous Slab Casting Mold. Thomas, Brain G, et al., et al. Urbana : ISIJ International, 2001, Vol. 41.
[20]. A Mechanism of Porosity Distribution in A356 Aluminum Alloy Castings. Li, Kun-Dar and Chang , Edward. S.l. : Materials Transaction, 2002, Vol. 43.
[21]. Vowell, Schuyler. Microfluidics : The Effect of Surface Tension. 2009.
[22]. Molina, J M, et al., et al. The Surface Tension of Liquid Aluminum in High Vacuum: The Role of Surface Tension. Alicante : s.n.
[23]. A Mechanism of Porosity Distribution in A356 Aluminum Alloy Castings. Li, Kun-Dar and Chang , Edward. 2002.
[24]. Surface Tension and Its Temperature Coefficient for Liquid Metals. Lu, H. M and Jiang, Q. s.l. : American Chemical Society, 2005.
[25]. A Unified Analysis of Filling and Solidification in Casting with Natural Convection. Im, Ik-Tae, Kim, Woo-Seung and Lee, Kwan-Soo. s.l. : Pergamon, 2001.
[26]. Randolph, Ransom &. Material Safety Data Sheet -Ranco Sil4.
[27]. Hadlegh Castings Aluminum Technology. Aluminum Casting Alloy.
[28]. Draft: Comparative Study of The Elastic Modulus of Various Periodic Lattice Structures Using Additive Manufacturing. Tan, Yu En, Moon, Seung Ki and Chua, Chee Kai. Oregon : ASME, 2013.
[29]. A multiple-gate runner system for gravity casting. Hsu, Fu-Yuan, Jolly, Mark R and Campbell, John. 2009, Journal of materials processing technology. 57

[30]. Gouldsen, Colin and Paul , Blake. Investment Casting Using FDM/ABS Rapid Prototype Patterns. s.l. : Stratasys Inc.

[31]. LTD, Objet Geometries. FullCure® Materials . s.l. : Objet Geometries LTD.

[32]. Systems, 3D. Visijet Materials for Projet HD & SD Printers. s.l. : 3D Systems.

[33]. Asadchii, O. G, et al., et al. Determination of tensile strength of paraffin wax. s.l. : Plenum Publishing Corporation.

[34]. Craig, R G, Eick, J D and Pevton, F A. Properties of Natural Waxes Used in Dentistry. Ann Arbor : University of Michigan, School of Dentistry.

[35]. Science Lab, Inc. www.Sciencelab.com. [Online]

[36]. A Novel hermetic differential scanning calorimeter (DSC) sample crucible. MacNeil, D D, et al., et al. s.l. : Elsevier, 2002, Vol. 386.

[37]. Morgan, Roger J and Ju, Jaehyung. Thermo-mechanical interface modeling of Chloro-Butyl Rubber stopper and Borosilicate glass vial.

.